A Numerical Study of the Effect of GOES Sounder Cloud-Cleared Brightness Temperatures on the Prediction of Hurricane Felix

XIAOLEI ZOU AND QINGNONG XIAO

Department of Meteorology, The Florida State University, Tallahassee, Florida

ALAN E. LIPTON AND GEORGE D. MODICA

Atmospheric and Environmental Research, Inc., Cambridge, Massachusetts

(Manuscript received 23 June 1999, in final form 20 March 2000)

ABSTRACT

The influence of Geostationary Operational Environmental Satellite (GOES) brightness temperature data on the numerical simulations of Hurricane Felix is investigated. Satellite data are included as an augmentation to a bogus data assimilation (BDA) procedure using a mesoscale adjoint modeling system. The assimilation of satellite data modified not only the environmental flow but also the structure of the initial vortex, which is located over a region devoid of satellite data. This modification resulted in a reduction of the 12-h forecast errors verified by radiosonde data. Despite the fact that the forecast using only the bogus surface low at the initial time was very good, track and intensity forecasts beyond 2 days of model integration were shown to be improved further by including satellite data in the initialization procedure. Differences in the prediction of Hurricane Felix with and without satellite data were also found in the prediction of the upper-level jet, the cold temperature trough ahead of the hurricane, the size of the hurricane eye, and the location of the maximum hydrometeor. Although the focus of this study is to assess the effect of the direct use of satellite brightness temperature data on hurricane prediction, it is also noted that the BDA experiment including only the bogus data shows a positive effect of the BDA vortex on the environmental flow during the forecast period, as verified by satellite observations.

1. Introduction

Initially designed for producing images of the earth's cloud cover, satellite instrumentation has been constantly improved to provide quantitative information about the atmosphere. Improvement of the large-scale analysis over data-sparse regions using satellite radiance data, for example, was reflected in an increased global forecast skill of operational numerical weather prediction in the Southern Hemisphere (Andersson et al. 1992; Eyre et al. 1993; Derber and Wu 1998). We therefore expect that satellite observations, which are now available at a resolution of about 30 km or higher, are important for hurricane modeling, given that the routine rawinsonde and ship data are too sparse to capture many important mesoscale features in the initial conditions for hurricane simulation. Initialization for hurricane prediction will become an even more serious problem with the rapid increase in model resolution for hurricane simulation. Several studies investigated the effect of satellite-retrieval products (such as rain rate) on hurricane initialization and prediction (Krishnamurti et al. 1995; Peng and Chang 1996; Karyampudi et al. 1998; Xiao et al. 2000). Satellite observations in these studies were incorporated into the forecast model through various kinds of reverse cumulus parameterization procedures. The effect of the direct use of satellite brightness temperatures, instead of their retrieved products, needs to be assessed.

The work summarized in this paper presents part of the effort funded by the Air Force Office of Scientific Research (AFOSR) to assess the effect of Geostationary Operational Environmental Satellite (*GOES-8*) brightness temperature data on hurricane prediction. The case chosen for this study is Hurricane Felix from the 1995 Atlantic hurricane season, which lasted from 12 to 21 August 1995. During the preprocessing of *GOES-8* brightness temperature data, the cloudy hurricane region was avoided because data in these areas are likely to be contaminated by cloud uncertainties. In other words, we applied a cloud-clearing step in preparing the satellite data. Because of lack of data over the hurricane region, a bogus vortex initialization is needed for a successful

Corresponding author address: Xiaolei Zou, Dept. of Meteorology, The Florida State University, 404 Love Bldg., Tallahassee, FL 32306-4520.
E-mail: zou@met.fsu.edu

TABLE 1. Radiative-transfer model layers [fixed pressure levels (hPa)].

0.1	0.2	0.5	1.0	1.5	2.0	3.0	4.0	5.0	7.0
10.0	15.0	20.0	25.0	30.0	50.0	60.0	70.0	85.0	100.0
115.0	135.0	150.0	200.0	250.0	300.0	350.0	400.0	430.0	475.0
500.0	570.0	620.0	670.0	700.0	780.0	850.0	920.0	950.0	1000.0

hurricane simulation and for a proper assessment of the effect of the *GOES-8* satellite data. To allow the direct use of satellite observations in the hurricane initialization, we developed a variational bogus data (BDA) scheme in which a bogus surface low is introduced simultaneously with brightness temperature observations into a four dimensional variational data assimilation procedure. Some technical details and numerical results of the BDA hurricane initialization procedure can be found in Zou and Xiao (2000). It was shown that an initial condition of all model variables can be generated by fitting the forecast model to a bogus surface low that is specified based on a few observed and estimated parameters. As a result of BDA, dramatic improvements occurred in the simulation of the track, intensity, and structure of Hurricane Felix. The current paper demonstrates the feasibility of including satellite brightness temperature observations directly into the BDA procedure and of assessing the potential effect of environmental satellite data on hurricane prediction. We first developed the techniques necessary to incorporate the satellite data into a hurricane prediction model. This necessitated the development of the adjoint of a radiative transfer model and the proper linkage of both the radiative transfer model and its adjoint into the MM5 adjoint model system (Zou et al. 1995, 1997). We then assessed the effect of satellite data available in the surrounding environment of the hurricane for the simulation of hurricane track and intensity changes during the period from 1200 UTC 15 to 0000 UTC 19 August 1995, during which Felix made a northeastward recurvature from its northwestward track.

The paper is arranged as follows. In section 2, we provide a brief description of *GOES-8* brightness temperature measurements, the radiative transfer model, the quality control, and the measurement errors. Section 3 reports the sensitivities of brightness temperatures at different channels to several assigned temperature and humidity profiles. The data assimilation procedure, forecast model, and experiment design are presented in section 4. In section 5, the model initial conditions obtained by the BDA scheme with assimilation of *GOES-8* brightness temperatures are described and compared with those without assimilation of *GOES-8* brightness temperatures. The effect of the bogus surface pressure and *GOES-8* cloud-free brightness temperatures on the simulation of hurricane Felix is presented in section 6. The paper concludes in section 7.

2. *GOES-8* satellite data and a radiative transfer model

a. A brief description of GOES-8 *satellite data*

The new series of Geostationary Operational Environmental Satellites beginning with *GOES-8* was launched on 13 April 1994. It has been designed with separate imaging and sounding instruments to support the requirements of the modernized National Weather Service. It is three-axis stabilized to improve instrument performance and to enable more efficient data gathering by both the imager and sounder. The *GOES-8* sounder includes 18 thermal infrared bands plus a low-resolution visible band. The spectral bands are sensitive to temperature, moisture, and ozone. Significant improvements in data quality and information content, with respect to previous geostationary satellites, encourage the use of these data in many areas of research (Smith and Lee 1995).

The potential use of satellite data to contribute significantly to hurricane forecasting, for which models are initialized mostly over oceanic regions, needs to be assessed fully. However, the ''optimal'' use of satellite data faces many challenges. Among these are (i) the quality control of the observed brightness temperatures to remove potentially cloud-contaminated or erroneous data and (ii) the direct use of brightness temperature data instead of the retrieval products. The latter requires a computationally efficient radiative transfer model that computes the brightness temperatures from the meteorological variables. One such radiative transfer model for the use of *GOES-8* brightness temperatures is briefly illustrated in the following section.

b. Radiative transfer model

In this research, we adopted a radiative transfer model similar to that of Eyre and Woolf (1988) and Eyre (1991), with some modifications made to fit the *GOES-8* sensor observation. The input variables of our radiative transfer model are temperature and relative humidity profiles, surface pressure, and surface skin temperature. The forward model consists of 40 layers ranging from 0.1 to 1000 hPa (Table 1). Because the radiative-transfer model layers are not necessarily consistent with the model layers for which values of temperature and humidity are available, interpolation or extrapolation of pressure p is needed. In this study, a linear interpolation (extrapolation) scheme in $\log(p)$ is adopted to generate temperature and humidity in the 40 radiative-transfer

model layers from the 27 σ-layer model analysis and/or forecast, where $\sigma = (p - p_t)/(p_s - p_t)$, with p_s being surface pressure and p_t being pressure at the model top.

The fast transmittance model developed by Eyre and Woolf (1988) is used to calculate the transmittance of the atmosphere. For *GOES-8*, every individual field of view (IFOV) has a unique zenith angle. The transmittance coefficients are found by multiple regression, which fits to the line-by-line radiative transfer model (LBLRTM; see Clough et al. 1992), and are supplied as constant quantities to our radiative transfer model.

The radiance R_α is then calculated within the integration of a radiative transfer equation (Liou 1980). For infrared channels, the clear-column radiance of channel α is given by

$$R_\alpha = R_\alpha^s + R_\alpha^u + R_\alpha^d, \quad (1)$$

where R_α^s is the contribution from the surface, R_α^u is the contribution from atmospheric direct upward emission, and R_α^d is the contribution from atmospheric downward emission reflected back from the surface, which was neglected in this study.

The surface contribution is given by

$$R_\alpha^s = \varepsilon_\alpha B_\alpha(T_s)\tau_\alpha(p_s), \quad (2)$$

where ε_α denotes surface emissivity at frequency α, B_α is the Planck function, T_s is surface temperature, and $\tau_\alpha(p_s)$ is the transmittance from the earth's surface to space. Over land, the surface emissivity ε_α was assumed to be 0.97 for channels 1–12 and 0.96 for channels 13–18. Over ocean, the surface emissivity was 0.98 for all channels. The numbers are based on empirical experience with the GOES visible–infrared spin scan radiometer atmospheric sounder, comparing observed brightness temperatures with computed values. The values are within the range of values that have been measured or computed for each surface material (Liu et al. 1987; Masuda et al. 1988; Sutherland 1986).

The contribution of direct atmospheric upward emission is obtained as a sum of the contributions from all emitting layers:

$$R_\alpha^u = \frac{1}{2}\sum_{k=1}^{N}[B_\alpha(T_k) + B_\alpha(T_{k-1})][\tau_{\alpha,k-1} - \tau_{\alpha,k}], \quad (3)$$

where T_k is the temperature at atmospheric level k and $\tau_{\alpha,k}$ is the transmittance in channel α from level k to space. The brightness temperature is converted from radiance using the inverse Planck function.

c. Data quality control and error statistics

Infrared satellite data were collected at the Air Force Research Laboratory (AFRL) from the sounder aboard the *GOES-8* satellite using the AFRL Interactive Meteorological System facility. The *GOES-8* sounder data were cloud cleared to correct for the complicating effects that hydrometeors have on the interpretation of infrared brightness temperatures. Cloudy *GOES-8* IFOVs were identified using a person–computer interactive cloud–clear discrimination program that operated on images made with data from the visible channel and from the infrared channels at 3.7 and 11.0 μm. To create a single sounding field of view (SFOV), a set of IFOVs were averaged horizontally. The purpose of the averaging is to compensate for data noise. We used the method outlined in Lipton (1998) to select a set of averaging areas that would minimize the gaps in coverage caused by clouds. Data were averaged from 3×3 boxes of *GOES-8* IFOVs, resulting in SFOVs that represent an area of approximately 30×30 km^2. At least four clear IFOVs were required to make an SFOV, and an isolation limit of nine clear IFOVs was used.

TABLE 2. Table of errors for the *GOES-8* satellite radiance.

Channel	Wavenumber (cm^{-1})	Wavelength (μm)	E_{ins} [mW (m^2 sr cm)$^{-1}$]	E_{fwd} [mW (m^2 sr cm)$^{-1}$]
1	680.71	14.71	1.030	0.036
2	695.73	14.37	0.790	0.028
3	711.88	14.06	0.720	0.124
4	732.50	13.96	0.640	0.159
5	747.53	13.37	0.560	0.183
6	790.40	12.66	0.340	0.250
7	829.07	12.02	0.320	0.228
8	906.55	11.03	0.250	0.188
9	1029.55	9.71	0.190	0.539
10	1339.55	7.43	0.130	0.111
11	1422.01	7.02	0.073	0.110
12	1535.43	6.51	0.104	0.054
13	2184.93	4.57	0.013	0.022
14	2207.49	4.52	0.008	0.012
15	2247.11	4.45	0.009	0.003
16	2421.74	4.13	0.005	0.036
17	2509.51	3.98	0.007	0.012
18	2666.41	3.74	0.006	0.001

After the cloud- and precipitation-clearing steps outlined above, the satellite data were further processed by removing the bias between the satellite brightness temperatures and those calculated from collocated radiosonde observations. For this step, we used a shrinkage estimator (Fleming et al. 1991), which is a modified regression technique. In our application of the shrinkage estimation technique, we used the satellite sounder channels, the latitude, and the satellite zenith angle of the satellite observations as predictors. The radiosonde–*GOES-8* observation pairs were taken from 1200 UTC 15 and 0000 UTC 16 August 1995. The approximate region was from about 24.56° to 42.59°N and 72.66° to 89.31°W. Table 2 gives the *GOES-8* instrument noise errors E_{ins} and the forward model errors E_{fwd}. Values of E_{ins} were computed using a statistical data analysis method (Hillger and Vonder Haar 1988). The forward model errors E_{fwd} were evaluated from comparison between the ''fast'' forward model and the slow LBLRTM. The error variances of *GOES-8* radiance for each channel are then calculated by

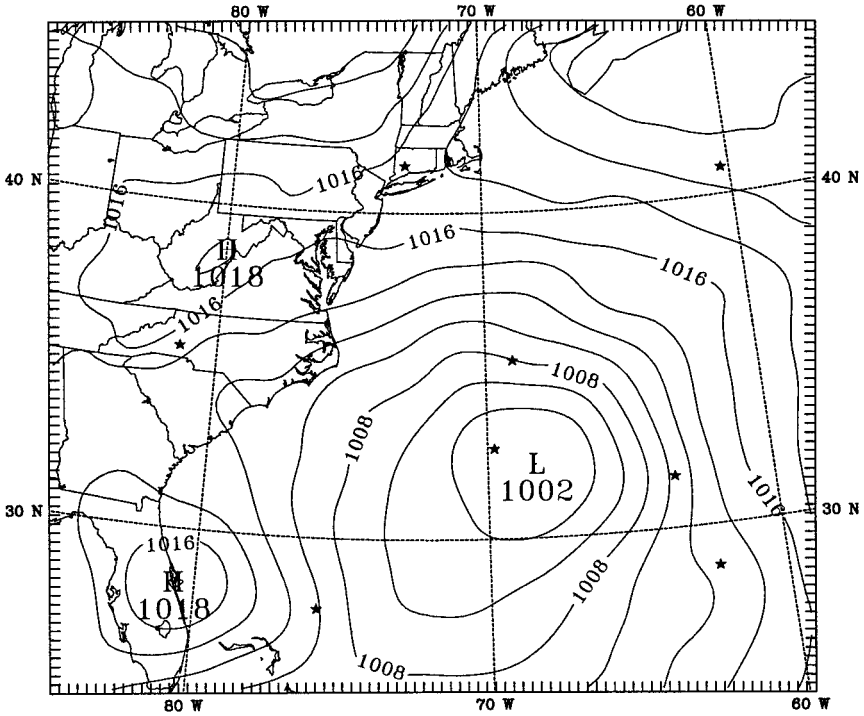

FIG. 1. NCEP sea level pressure analysis enhanced by MM5 preprocessing procedure at 1200 UTC 15 Aug 1995. The stars indicate locations at which the adjoint sensitivities of the *GOES-8* brightness temperatures were calculated.

$$\text{Var} = E_{\text{fwd}}^2 + \frac{E_{\text{ins}}^2}{n}, \tag{4}$$

where n is the number of samples averaged for the given IFOV. The error variance of brightness temperature is computed by multiplying the radiance error variance by $(dT_b/dR)^2$, which is the derivative of the brightness temperature T_b with respect to radiance based on the Planck function.

3. Sensitivity analysis of brightness temperatures with respect to temperature and specific humidity profiles

GOES-8 sounders measure brightness temperatures from 18 infrared spectral bands that are sensitive to the atmospheric temperature and moisture at various heights. To assess the sensitivity of the brightness temperatures with respect to perturbations in different atmospheric states, adjoint sensitivity analysis was performed. A simple response function was defined as

$$J_\alpha = J_\alpha(T, q, T_{\text{sk}}, p_s) = T_b(\alpha), \tag{5}$$

where $T_b(\alpha)$ is the brightness temperature at the α channel, T is the temperature, q is the specific humidity, and T_{sk} is the surface skin temperature. In our study, T_{sk} is fixed and all the others (T, q, and p_s) are taken as input variables to the radiative transfer model and will be represented by the vector $\mathbf{x}$.

The sensitivity of J_α with respect to $\mathbf{x}$, expressed as VJ, is usually defined as

$$VJ_\alpha(\mathbf{x}, \Delta\mathbf{x}) = (\nabla J_\alpha)^{\text{T}}\Delta\mathbf{x} \equiv (\hat{\mathbf{x}})^{\text{T}}\Delta\mathbf{x}, \tag{6}$$

where $\hat{\mathbf{x}}$ is the result of the adjoint model integration with a unit input for the adjoint variable of the brightness temperature at channel α, and zero value for the adjoint brightness temperature variables at other channels.

If a variation occurs solely in the lth component of the control variable vector $\mathbf{x}$, we denote by $\Delta\mathbf{x}^l$ the corresponding vector of variation:

$$\Delta\mathbf{x}^l = (0, \ldots, \Delta x^l, \ldots, 0)^{\text{T}}, \tag{7}$$

and denote the corresponding sensitivity by VJ_α^l. The relative sensitivity S_α^l is defined as the nondimensional quantity (Zou et al. 1993)

$$S_\alpha^l = \frac{VJ_\alpha^l}{J_\alpha}\left(\frac{\Delta x^l}{x^l}\right)^{-1}. \tag{8}$$

The magnitude of the relative sensitivity serves as a guide to ranking the importance of different components in the input variables $\mathbf{x}$. A plot of the vertical profile of the relative sensitivity, for example, will indicate where the most sensitive ranges of height are for brightness temperature information available at a certain channel.

Figure 1 shows the distribution of the sea level pressure (SLP) at 1200 UTC 15 August 1995 from the National Centers for Environmental Prediction (NCEP)

analysis enhanced by the Fifth-Generation Pennsylvania State University–National Center for Atmospheric Research Mesoscale Model (MM5) data preprocessing procedure. At this time, Hurricane Felix (1995) was located off the east coast of the United States over the ocean. We randomly selected eight points inside and outside the hurricane (''star'' in Fig. 1 denotes the points that were selected). The relative sensitivities of the brightness temperatures with respect to temperature and humidity profiles at these eight points were calculated. Numerical results showed that the sensitivity profiles for the same channel have, in general, similar variations with height for all the soundings selected, although these eight points represent different atmospheric profiles. Figure 2 depicts the relative sensitivities of the brightness temperatures at various channels, averaged over the eight selected soundings. An important feature is that sensitivities of brightness temperatures to temperature are positive at all channels (Fig. 2). The warmer the atmosphere is, the larger the brightness temperature is. The sensitivity to temperature is not uniform at different levels, and the level at which the brightness temperature is most sensitive varies with channels. The peak levels of relative sensitivity for channels 1, (14.71 μm), 2 (14.37 μm), 11 (7.02 μm), and 12 (6.51 μm), are above or near 300 hPa. Channel 3 (14.06 μm) has a peak at 350 hPa. For channels 4 (13.96 μm), 5 (13.37 μm), and 10 (7.43 μm), the largest sensitivities occur at midtroposphere. The brightness temperatures at channels 6–9, 13–14, and 16–18 are most sensitive to temperatures in the low troposphere. Most midwave band channels (channels 13–18 with 4.57 to 3.74 μm) show the largest sensitivity of the brightness temperatures to the temperature at low levels except channel 15. Sensitivities of brightness temperatures with respect to moisture profiles are negative at all channels (Fig. 2, dashed lines). In other words, the more moist the atmosphere, the lower is the *GOES-8* satellite-detected brightness temperature. The level of the largest sensitivities of the brightness temperatures are in the low troposphere at channels 6–9, 13–14, and 16–18 and the upper troposphere at channels 10–12. Very small water vapor sensitivities are observed for channels 1–4 and 15. These sensitivity analyses imply that observational information within the *GOES-8* brightness temperatures is likely to have an effect on the atmospheric thermodynamic state at all levels.

4. Incorporating *GOES-8* brightness temperatures into the BDA hurricane initialization scheme

a. Cost function formulation and the two BDA experiments

There were 12 time levels when *GOES-8* brightness temperature observations were available in the 6-h window from 1200 UTC to 1800 UTC 15 August 1995. Specifically, the *GOES-8* observations were collected at time $t_n = t_0 + \Delta t_n$, where $\Delta t_n = 0$, 46, 88, 107, 148, 167, 208, 226, 268, 287, 328, and 346 min and t_0 corresponds to 1200 UTC 15 August 1995. Figure 3a plots the locations of all the brightness temperature observations that were available over the assimilation domain during the 6-h time window, for incorporation into the BDA procedure. Satellite data were available over most areas except the initial vortex region. To assess the effect of these satellite data on the 2–3-day prediction of the hurricane, an initial bogus vortex was needed to compensate for the satellite data void over the initial vortex region as mentioned earlier. We thus developed, as the first step, a variational bogus data assimilation scheme that makes use of a bogus surface low. The BDA scheme and its numerical performance on the initialization of Hurricane Felix at a mature stage and the subsequent prediction were presented in Zou and Xiao (2000). In the study reported here, we included the satellite data into the BDA procedure. The bogus surface low was specified using the Fujita formula with the observed central value of SLP and the estimated radius of maximum low-level wind as the input to the axisymmetric vortex.

The four-dimensional variational data assimilation experiments were carried out by minimizing two cost functions: one is $J_{\rm bg}$, which measures the discrepancy between the model-predicted and specified sea level pressures representing the bogus surface low, and the other is $J_{\rm bgsat}$, in which an additional term is added to $J_{\rm bg}$ to minimize also the distance between model-predicted and *GOES-8* observed brightness temperatures. A simple background term J_b is included in both cost functions. Mathematically, they can be expressed as

$$J_{\rm bg}(\mathbf{x}_0) = \sum_{t_m} \sum_{i,j \in \mathcal{R}} (P - P^{\rm bogus})^{\rm T} W_P (P - P^{\rm bogus}) + J_b \quad \text{and} \tag{9}$$

$$J_{\rm bgsat}(\mathbf{x}_0) = \sum_{t_n} \sum_{\mathbf{r}_k} (T_b - T_b^{\rm GOES-8})^{\rm T} W_{\rm bt} (T_b - T_b^{\rm GOES-8}) + J_{\rm bg}, \tag{10}$$

where

$$J_b(\mathbf{x}_0) = \frac{1}{2}(\mathbf{x}_0 - \mathbf{x}_b)^{\rm T} W_b (\mathbf{x}_0 - \mathbf{x}_b). \tag{11}$$

Here, the summation over t_m in (9) was carried out over a one-half-hour window at 5-min intervals starting from t_0 (1200 UTC 15 August 1999). Here, $\mathcal{R}$ is a two-dimensional circular domain of 300-km radius centered at the hurricane center, and (i, j) represent model horizontal grid points within $\mathcal{R}$ at the lowest σ level ($\sigma = 0.995$). The cost function $J_{\rm bgsat}$ was calculated over a 6-h window. The summation in (10) was carried out at t_n, which represents the 12 observational times $t_n = t_0 + \Delta t_n$, where $\Delta t_n = 0$, 46, 88, 107, 148, 167, 208, 226, 268, 287, 328, and 346 min. The vector $\mathbf{r_k}$ represents the physical locations of all *GOES-8* brightness tem-

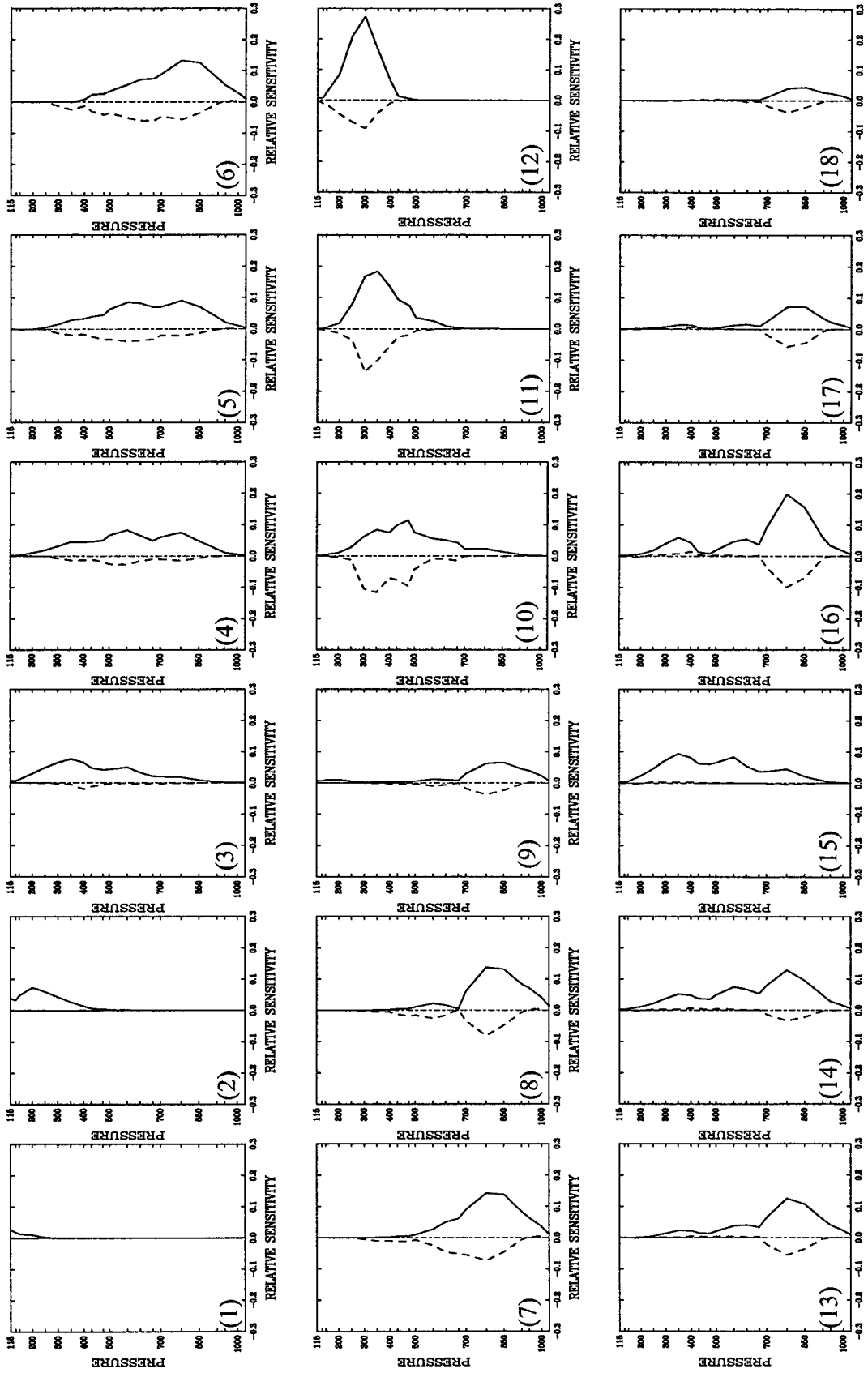

FIG. 2. Averaged relative sensitivities of the brightness temperatures at all of the 18 channels with respect to temperature (solid lines) and humidity (dashed lines) profiles. The average is taken over all eight selected points.

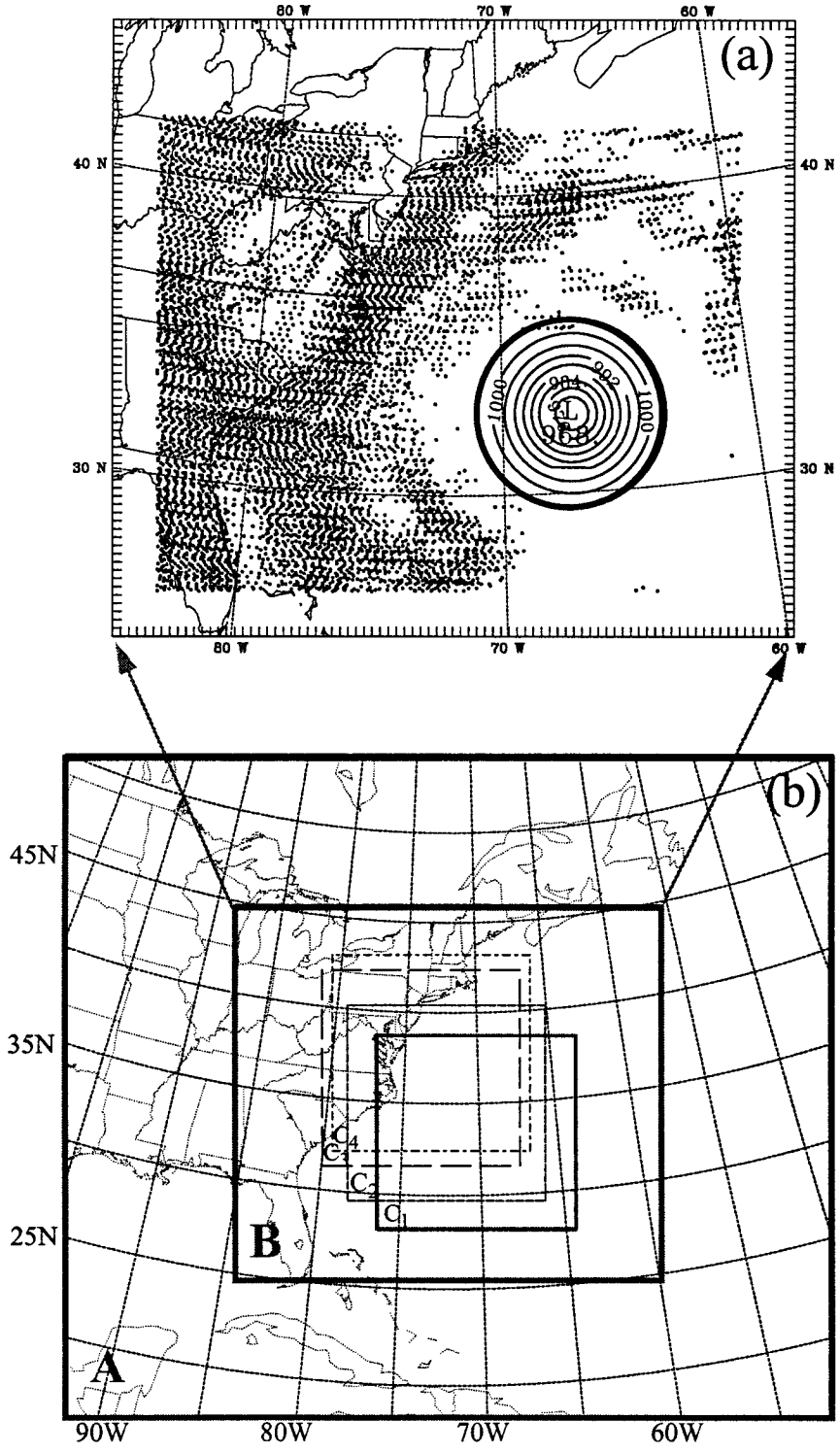

FIG. 3. (a) Locations of all the brightness temperature observations (dots) that were available from 1200 to 1800 UTC 15 Aug 1995. The thick isolines show the distribution of the bogus sea level pressure of the initial hurricane vortex. (b) The three model domains used for the forecast experiments.

peratures at time t_n. Variables P and T_b represent the sea level pressure and brightness temperature, respectively. Here, J_b is a simple background term measuring the distance between the model state ($\mathbf{x}_0$) and the MM5 analysis based on the large-scale NCEP analysis ($\mathbf{x}_b$). Both J_{bg} and J_{bgsat} are functions of the model initial condition $\mathbf{x}_0$. During the minimization procedure, $\mathbf{x}_0$ is adjusted to fit the model solution to the bogus surface low and/or the *GOES-8* brightness temperatures as closely as possible. The values W_P, W_{bt}, and W_b are diagonal weighting matrices approximating the error variances of the bogus surface low, the brightness temperature data, and the background estimate of the model state, respectively. The value of W_P was taken simply as a constant and was determined empirically by assuming a 1-hPa pressure error. Here, W_{bt} was calculated based on the error statistics of the *GOES-8* brightness temperatures, the error variance of which was computed by multiplying the radiance error variance [see (4) and Table 2] by $(dT/dR)^2$, where dT/dR is the derivative of the temperature with respect to the Planck function. The value of W_{bt} is the inverse of the brightness temperature error variance Var. For the background term, the value of the weighting W_b was calculated as the inverse of the maximum differences at each vertical level of two MM5 analyses 12 h apart.

All the data assimilation experiments were carried out at 30-km horizontal spacing using the adjoint modeling system of MM5 described by Zou et al. (1997, 1998). The physical parameterizations included in the minimization program of the model were (i) a bulk aerodynamic formulation of the planetary boundary layer, (ii) a dry convective adjustment, (iii) grid-resolvable large-scale precipitation, and (iv) the Kuo cumulus parameterization scheme.

b. The forecast model

A version of the MM5 nonhydrostatic, movable, and triply nested grid model version was used for the 3.5-day numerical simulation of Hurricane Felix. The grid system contained the triply nested meshes and 27 σ layers for all grid meshes, with horizontal spacing of 90 km for the coarse domain A, 30 km for the intermediate domain B, and 10 km for the fine-mesh domain C (see Fig. 3b for the domain configuration). The 27-layer σ values are 0.025, 0.070, 0.110, 0.150, 0.190, 0.230, 0.270, 0.310, 0.350, 0.390, 0.430, 0.470, 0.510, 0.550, 0.590, 0.630, 0.670, 0.710, 0.750, 0.790, 0.830, 0.870, 0.910, 0.945, 0.970, 0.985, and 0.995. The horizontal dimensions for domains A, B, and C were 45 $\times$ 51, 76 $\times$ 85, and 121 $\times$ 121, respectively. Domains A and B were fixed throughout the simulation, and the 10-km domain C_i moved along the hurricane track, with domains C_1, C_2, C_3, and C_4 used for the forecast periods of 0–18 h, 18–42 h, 42–55 h, and 55–84 h, respectively.

The model's moist processes included parameterization of shallow convection for all domains, Grell cumulus parameterization and stable precipitation scheme for domain A, Grell cumulus parameterization and Dudhia's simple-ice explicit moisture scheme for domain B, and Kain–Fritsch cumulus parameterization and mixed-phase explicit moisture processes for domains C_1, C_2, C_3, and C_4. The high-resolution planetary boundary layer parameterization scheme (Blackadar scheme) was used for all the domains. The land surface temperature was calculated using surface energy budget equations. For a more detailed description of MM5, see Dudhia (1993) and Grell et al. (1994).

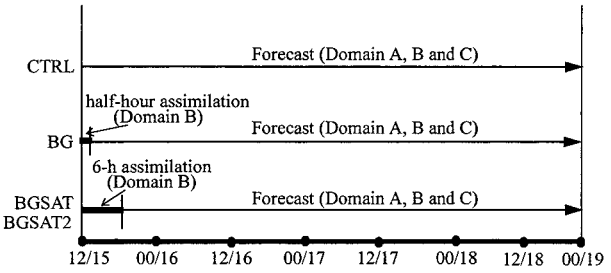

FIG. 4. Experiment design indicating the time windows of the data assimilation and the subsequent model forecast.

c. Experiment design

We conducted four forecast experiments, all initialized at 1200 UTC 15 August 1995 (Fig. 4). This time period is when Hurricane Felix was approaching the Outer Banks of North Carolina. The National Hurricane Center official operational track forecast indicated that Felix would make a landfall in 72 h from the initial time.

The same model configuration, described in section 4b, was used for all four forecast experiments. Only the initial conditions were different. The initial condition obtained by the standard preprocessing procedure of MM5 (Grell et al. 1994) was used as the initial condition for the control experiment CTRL. The initial condition obtained with the use of bogus surface data through minimizing J_{bg} was used as the initial condition for the BG experiment. The initial conditions obtained with the use of both bogus surface data and satellite brightness temperature data through minimizing J_{bgsat} were used as the initial conditions for the two experiments BGSAT and BGSAT2. Only those *GOES-8* brightness temperatures with values that differed from that of the large-scale analysis by less than 2°C (4°C) were included in the data assimilation procedures of BGSAT (BGSAT2).

The bogus and satellite data assimilation experiments were carried out on a single domain, domain B, at 30-km spacing over one-half-hour (for BG) and 6-h (for BGSAT and BGSAT2) windows, respectively. The initial conditions on domain C_1 at 10-km spacing were obtained from the initial conditions at 30 km by a linear interpolation. The initial conditions for domain A at 90 km were obtained from the NCEP large-scale analysis.

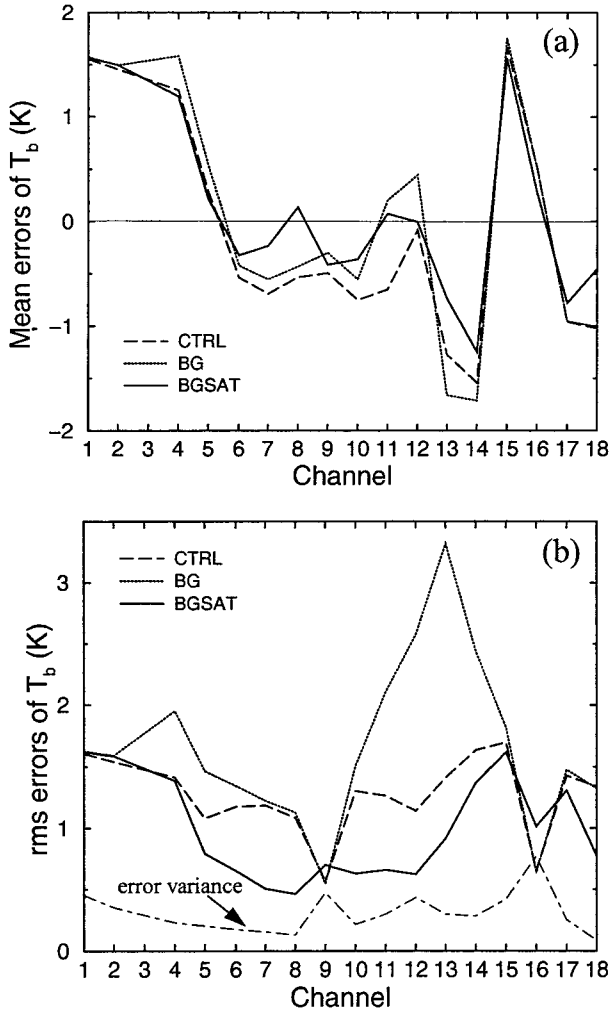

FIG. 5. (a) The mean error and (b) the rms errors of brightness temperatures for CTRL (dashed line), BG (dotted line), and BGSAT (solid line), verified by all *GOES-8* satellite observations available within the assimilation window. Also shown in (b) are the observational error variances at different channels (dash–dotted line).

5. Numerical results from BDA with and without *GOES-8* brightness temperatures

a. The fit to data

To see how well the model fits to the *GOES-8* brightness temperature data, we plot in Fig. 5 the mean errors and the rms errors between the simulated and the observed *GOES-8* brightness temperatures for CTRL (dashed line), BG (dotted line), and BGSAT (solid line). The mean errors and the rms errors were calculated for all the *GOES-8* observations available in the 6-h time window (from 1200 to 1800 UTC 15 August 1995). The mean errors were reduced for all channels after data assimilation (Fig. 5a). Large error reductions in terms of distance of the analysis of BGSAT to the satellite observations occur mainly in the channels 5–8 and 10–15. As we know from the sensitivity profile (Fig. 2), large sensitivities of the brightness temperatures at channels 5–8 and 13–14 are found in the low troposphere for both the temperature and the specific humidity fields. The brightness temperatures at channels 10–12 and 15 are more sensitive to the temperature and specific humidity in the mid- and upper troposphere. The fit of the model state to observations at channels 9 and 16 is slightly degraded after data assimilation. The problem of the satellite data assimilation at channels 9 and 16 is found to be linked to the large observational error variances at these two channels (see the dash–dotted line in Fig. 5b). During the model fit to the specified bogus surface low, adjustments occurred outside the vortex region that resulted in larger rms errors for the BG analysis than for the background field in comparison with the *GOES-8* observations.

TABLE 3. The fit of the model forecasted state to *GOES-8* brightness temperatures [the rms errors between the simulated and observed T_b (unit: K)].

	T_b observational times					
Experiment	1846 UTC (837*)	1947 UTC (796)	2047 UTC (916)	2147 UTC (841)	2346 UTC (850)	Total (4240)
CTRL	1.69	1.64	1.65	1.64	1.73	1.67
BG	1.61	1.59	1.57	1.52	1.63	1.59
BGSAT	1.56	1.54	1.55	1.57	1.67	1.57

* The number of observational points.

It is logical to expect error reductions of the model solution when comparing it with data that were assimilated. What will be the fit of the model forecasts of, say BGSAT, to observations that are available beyond the assimilation time period? For Hurricane Felix, *GOES-8* brightness temperature data were also made available during the next 6-h period following the 6-h data assimilation window. These data exist at 10 time levels, with a total number of observations of 837, 140, 796, 148, 916, 151, 841, 106, 72, and 850 available, respectively, at 1846, 1928, 1947, 2028, 2047, 2129, 2147, 2229, 2328, and 2346 UTC 15 August 1995. At a few times when the available satellite data are less than 200 observations, the satellite data were located in the northeast corner of domain B, whereas at other times (5 out of 10) the data covered only the western half of domain B. Because the purpose is to assess the effect of upstream conditions on Hurricane Felix's track prediction, we calculated in Table 3 the fit of model forecasts to data at 1846, 1947, 2047, 2147, and 2346 UTC 15 August, when not only were the observations located upstream, but the number of observations was significantly larger (near or above 800). The brightness temperatures derived from the BGSAT model solution gave the best overall fit to the *GOES-8* satellite data. It is surprising to find that the fit of the BG forecast was generally slightly better than that of CTRL for the environmental flow prediction. Improvements in different channels for data at all the five time levels are shown

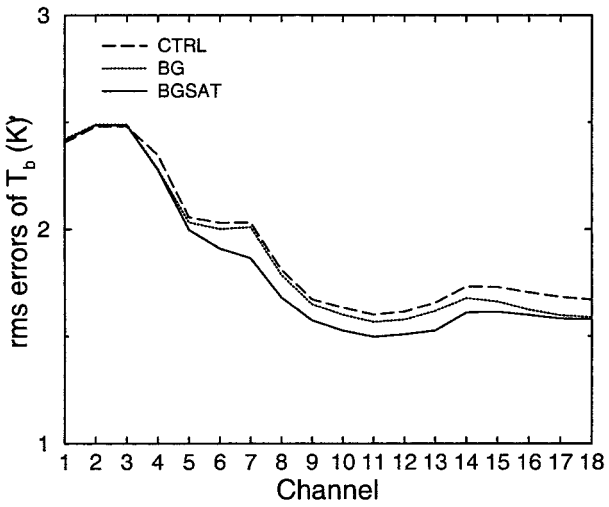

FIG. 6. Similar to Fig. 5b but for the 6-h forecast from 1800 UTC 15 Aug 1995. Only those observations at the five time levels at which the number of observations was large (close to 800) were included for the calculation.

in Fig. 6. Error reductions occurred for both BG and BGSAT for most channels during the forecast period from 6 to 12 h. The error reduction in the BG forecast indicates a positive effect of the BDA-generated hurricane on the simulation of environmental flow over the east coast and the eastern United States.

Model prediction contains errors of two kinds: errors in the initial condition and errors due to the imperfection of the forecast model. The fact that the forecast from BGSAT fits the *GOES-8* data better than does that of the BG beyond the assimilation window indicates that important adjustments in the model initial condition errors were made through satellite data assimilation, and these adjustments were significant enough to result in an improvement to the model simulation of Hurricane Felix beyond the assimilation window. Numerical results will be shown in more detail in the following two subsections.

b. *Differences in the initial conditions with and without the use of* GOES-8 *brightness temperatures*

As mentioned in sections 2 and 3, *GOES-8* brightness temperature information is directly sensitive to the atmospheric temperature and moisture fields. Figure 7 shows the mean and rms differences of the initial temperature and specific humidity fields between BGSAT and BG. The largest changes in the initial temperature field with the use of *GOES-8* brightness temperatures were near the surface and the top of the model (see solid line in Fig. 7b), with an increase of temperature in the low troposphere and a decrease of temperature in the mid- and upper troposphere (Fig. 7a). The relatively large changes in the temperature field near the model top, indicated by the rms difference, were found to be mainly over the vortex region. The mean and rms differences of the initial temperature fields between BGSAT and BG outside the vortex region (see the thick-line circle in Fig. 3a), shown in Fig. 7 as dash lines, confirm this result. The largest change in the initial moisture field was at $\sigma = 0.75$ (model level 19, near 800 hPa), with a dry bias below model level 14 and a small moist bias above level 14 but below level 7. Therefore, large changes to the initial condition describing the environmental flow outside the initial vortex region are found in all model levels for the temperature field and mostly in the low levels for the specific humidity field. A large difference between BG and BGSAT at a certain height implies that either the model is better fitted to brightness temperatures at those wave bands where the large sensitivity occurs at that height or the discrepancies between the background and the observations at these wave bands are larger than those at other wave bands. The former appears to be the case if we combine the results in Figs. 2 and 5. The fit of the model state to observations was best achieved for the brightness temperatures in channels 5–14 (Fig. 5b, solid curve) and the maximum sensitivities for the brightness temperatures at most of these channels are in the low troposphere (Fig. 2). The latter probably is not true, because the fit of the CTRL analysis to the observations (dashed line in Fig. 5b) does not show an absolute peak at the wave bands of 5–8 and 10–15.

In the following we first examine modifications made to the environmental flow by the assimilation of the *GOES-8* brightness temperatures and then examine the differences of the initial vortices obtained in BG and BGSAT. Comparing the surface temperature fields in BG and BGSAT (Fig. 8), we find that the two thermal ridges, one over the continent and the other over the ocean, are intensified after the assimilation of *GOES-8* brightness temperatures. The enhanced thermal ridges, as highlighted by 299- and 300-K contours, reflect the temperature adjustments to the initial condition as a direct result of fitting satellite brightness temperatures. The warm air to the west of the hurricane was allowed to penetrate farther north from the south. In the 850-hPa specific humidity field, the modification made to the background moisture field by satellite data was mostly negative to the west of the hurricane, indicating a reduced amount of moisture content after the assimilation (Fig. 9). The air to the west of the storm is drier in BGSAT by as much as 4 g kg^{-1} in comparison with that in BG.

The low-level temperature increase, corresponding to the intensified thermal ridge over the continent, was found to be associated with downward motions, which may have caused the subsidence warming. The region of maximum temperature increase is located to the west side of the Appalachian mountain ridge (Fig. 10). The representativeness of the real atmosphere is difficult to verify because of (i) very little or no independent ob-

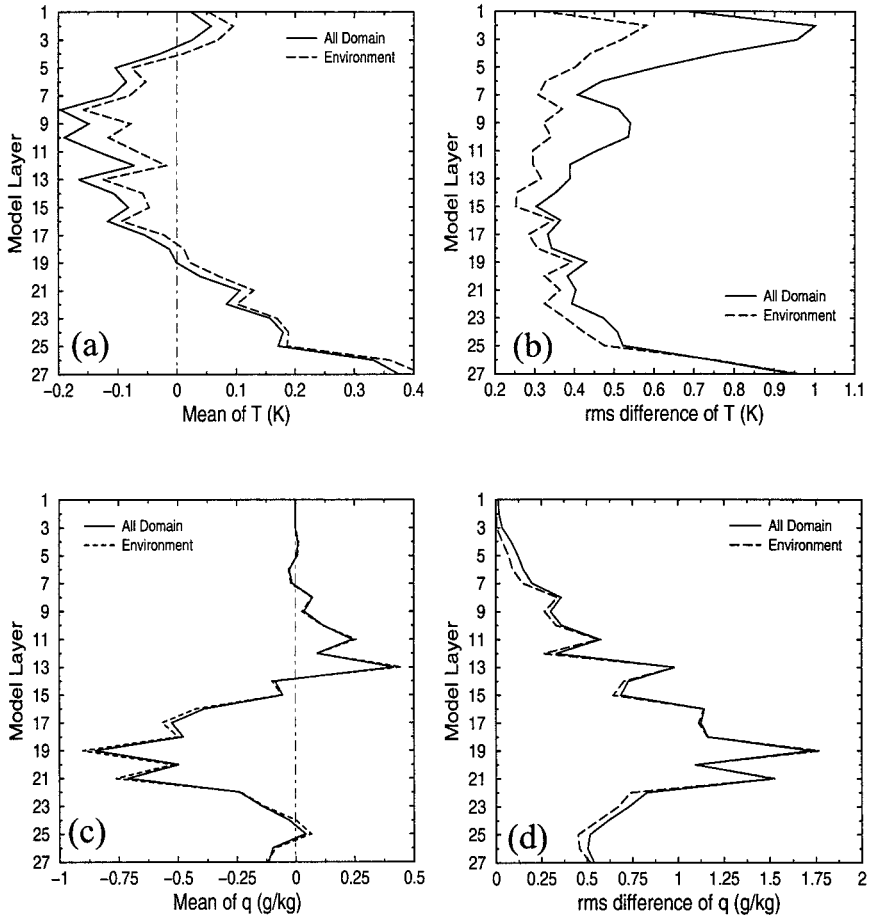

FIG. 7. The (left) mean and (right) rms difference of the initial differences in the (a)–(b) temperature and (c)–(d) specific humidity fields between BGSAT and BG. Solid lines are for entire domain B and dashed lines are for the environment region outside of the hurricane vortex region shown in Fig. 3a.

servations over these regions and (ii) the possible inclusion of model errors in the initial adjustments. During the fit to all brightness temperature observations in the 6-h assimilation window, errors may result from sources such as the imperfect forecast model, the approximated observation error variances, and the neglect of the observation error correlations. Nevertheless, we compared the model-derived profiles of temperature after the 12-h forecast with two radiosonde soundings that were available over these regions. The geographical locations of these two stations are shown in Fig. 10. Figure 11 shows the vertical profiles of the differences in temperature between the 12-h model results interpolated to the radiosonde stations A (at 38.4°N, 82.6°W: Huntington, West Virgina) and B (at 40.5°N, 80.2°W: Pittsburgh, Pennsylvania) and the radiosonde observations themselves (i.e., $T^{BG} - T^{OBS}$) for both BG and BGSAT. We find that the 12-h forecast errors are significantly reduced at most vertical levels because of the use of satellite data. The vertically averaged rms errors are shown in Table 4, including variables of temperature, zonal wind, meridional wind, and specific humidity. The assimilation of satellite brightness temperatures reduces the 12-h forecast errors of temperature and wind fields. Results for the specific humidity field are mixed at the two stations. We also compared the 12-h model forecasts to all of the radiosonde data in the forecasting domain B (a total of 23 stations), and an improvement in the 12-h forecast fit to data is observed (see Table 5).

Although there were no satellite observations over the vortex region at any time, differences in the initial conditions over the vortex region with and without *GOES-8* satellite data resulted from the interaction of the bogus surface low and the background flow, the latter being modified by the satellite data. For example, the low-level wind ($\sigma = 0.995$) distribution in the BG vortex is different from in the BGSAT vortex (Fig. 12). The maximum low-level winds are 36.7 and 53.6 m s^{-1} in BG and BGSAT, respectively. The latter may be too strong to be verified by observations. The maximum low-level winds in the BGSAT initial condition were located to the north of the vortex center, but they were

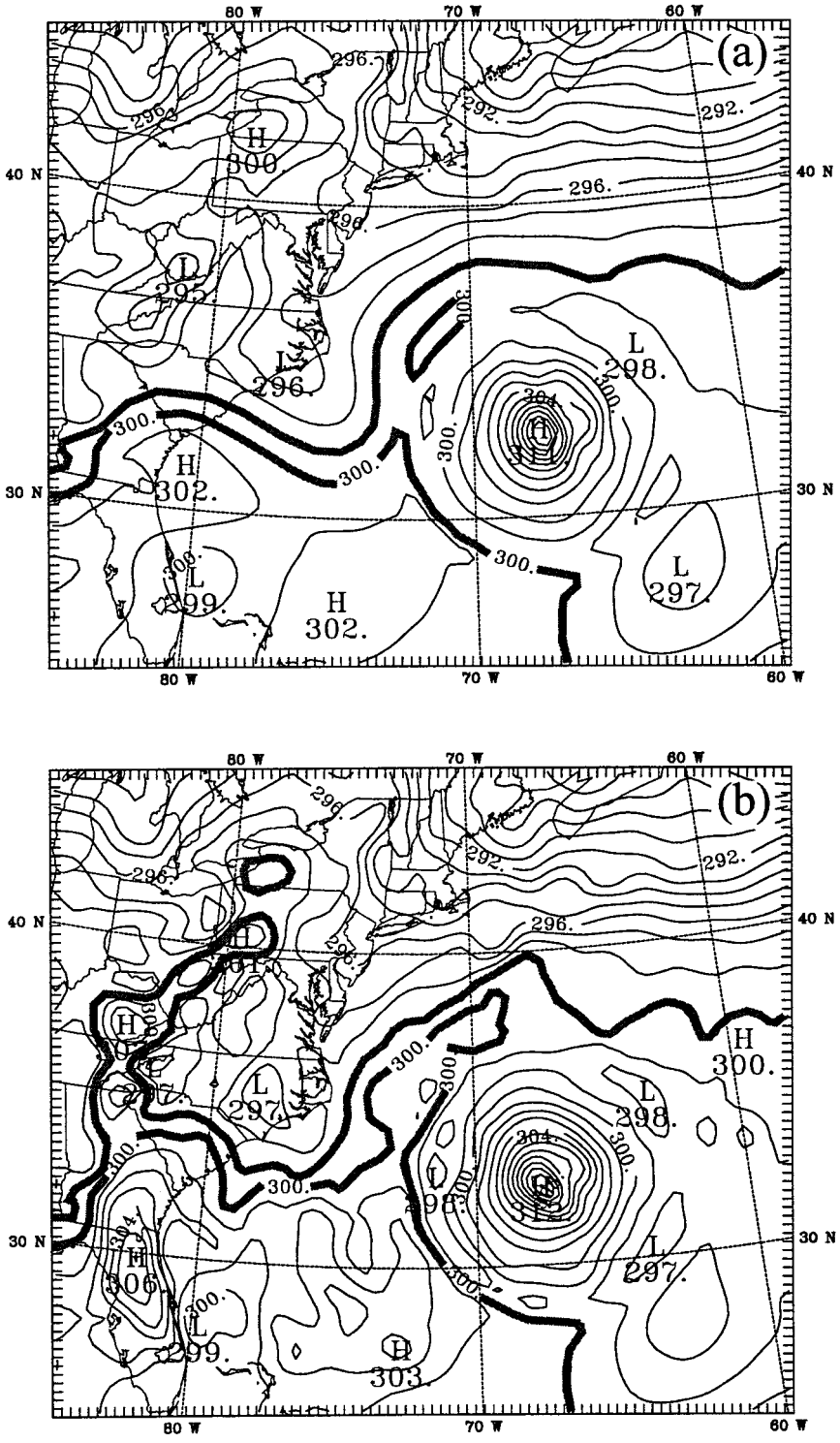

FIG. 8. Distributions of the initial surface temperature fields from (a) BG and (b) BGSAT. The contour interval is 1 K. The two thick lines are for the temperature at 299 and 300 K.

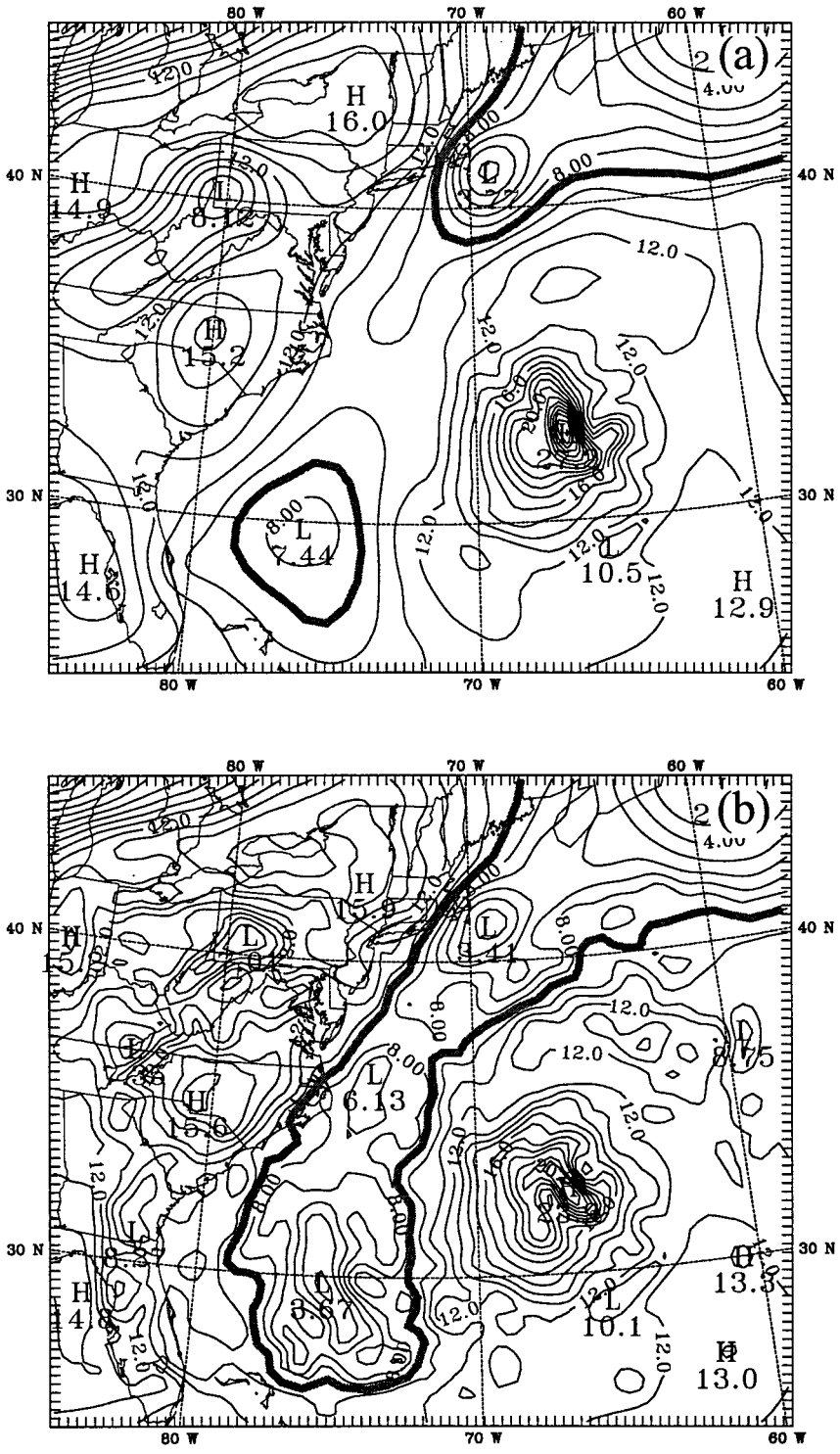

FIG. 9. Distributions of the initial specific humidity fields from (a) BG and (b) BGSAT. The contour interval is 1 g kg^{-1}. The thick line is for the specific humidity of 9 g kg^{-1}.

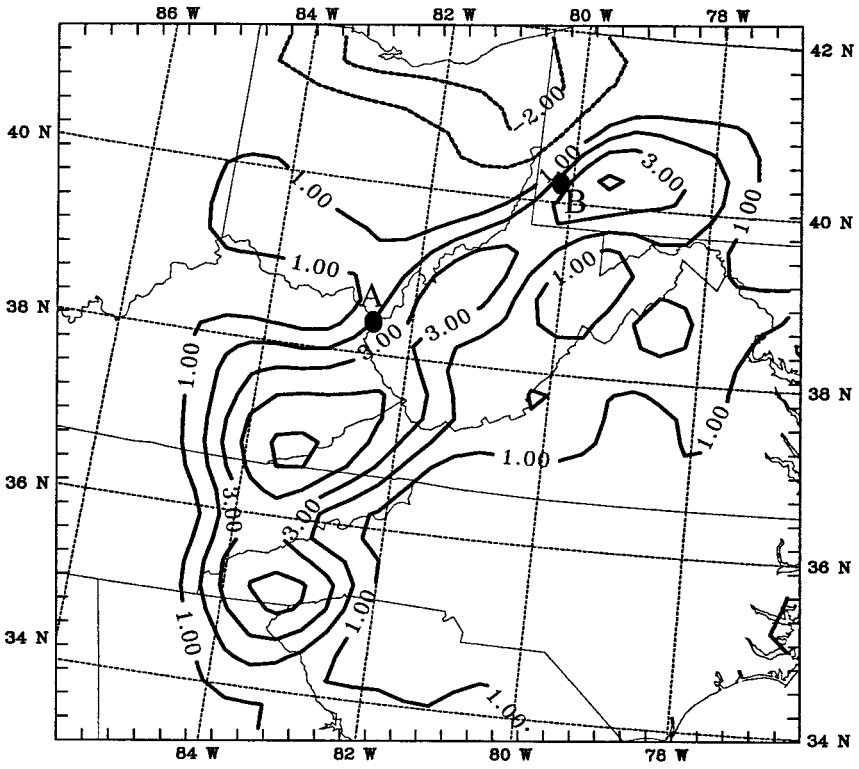

FIG. 10. Differences of the initial temperature between BGSAT and BG. The contour interval for the temperature is 1 K.

located to the east-northeast of the vortex center for BG. Differences arising from variations in the initial vortices of BG and BGSAT are also found in the other model fields (temperature, specific humidity, pressure perturbation, and vertical velocity). Because their distributions are mostly axisymmetric, we show in Fig. 13 a cross-section cutting through the initial vortex centers from west to east (along the line CD in Fig. 12). The adjustments of the temperature, specific humidity, pressure perturbation, and vertical velocity in BGSAT show more reasonable magnitudes than those from the BG assimilation. For example, the maximum temperature increase in the upper level of the BG vortex was as high as 26.3°C, but it was 14.7°C in the BGSAT vortex. The pressure increases in the upper levels above the surface low were 11.8 and 5.5 hPa for BG and BGSAT vortices, respectively. The vertical velocity on the east side of the BG vortex was greater than 600 cm s^{-1}; it was 135 cm s^{-1} in the BGSAT vortex. A temperature adjustment of 26.3°C and a vertical velocity of 600 cm s^{-1} in BG are difficult to verify through observations. The temperature increase seems to be related to the adiabatic warming associated with the descent in the eye. In addition, the air in the eye of the initial BGSAT vortex was drier than that in the BG vortex. The hurricane eye was generated in both BDA experiments, with descending warm and dry air in the center of the hurricane and ascending moist air around the eye throughout the entire layer of the model atmosphere. However, the BGSAT vortex is quantitatively more realistic than that of the BG vortex, except for too strong a surface wind in BGSAT.

Seeing the differences in both the environmental flow and the initial vortex described by the BG and BGSAT initial conditions, one compelling question would be what effect these differences have on the forecasts, or are they significant enough to make a difference in the subsequent 2–3 day prediction of Hurricane Felix? Results of the three model simulations using the NCEP analysis (CTRL), the BG initial condition, and the BGSAT initial condition are shown in the following section. Emphasis is placed on comparing numerical forecast results from BG and BGSAT.

6. Effect of satellite data on the simulation of Hurricane Felix

The effect of satellite data on the track and intensity forecast of Hurricane Felix is first assessed by comparing observations with the predicted hurricane positions, the central sea level pressures and the maximum low-level wind. Figures 14 and 15 show the track and intensity changes at 6-h intervals for the entire forecast period from 1200 UTC 15 to 0000 UTC 19 August 1995. Results from BGSAT2 were similar to those of BGSAT and are therefore not shown in these figures. The fore-

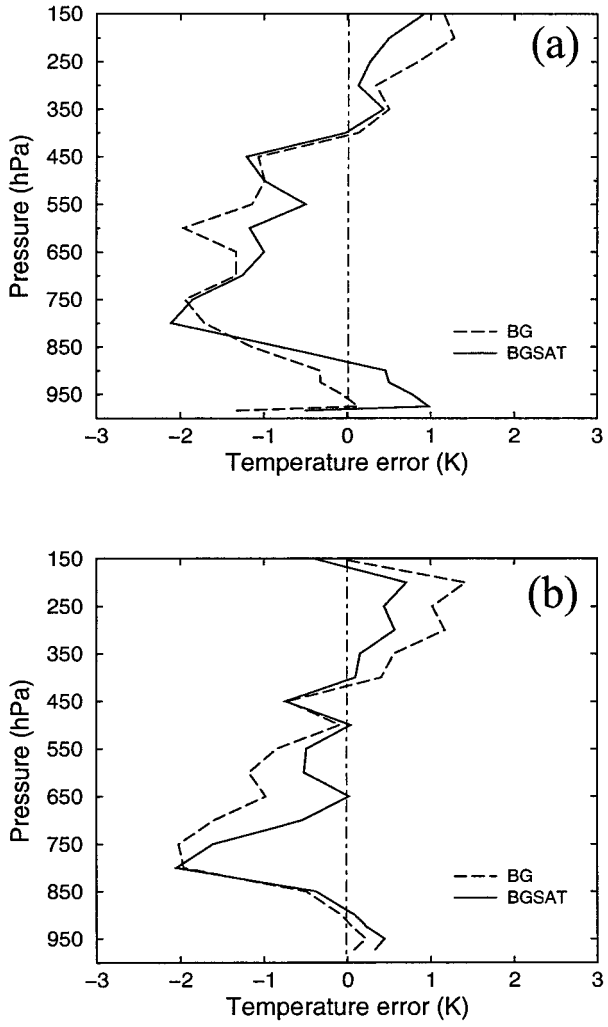

FIG. 11. The vertical profiles of the temperature differences between radiosonde observations and 12-h model results interpolated to the radiosonde stations at (a) Huntington, WV (38.4°N, 82.6°W) and (b) Pittsburgh, PA (40.5°N, 80.2°W) for both BG (dashed line) and BGSAT (solid line).

cast without data assimilation (CTRL) did reasonably well for the track prediction during the initial 36 h. However, it failed to predict a northeastward recurving movement of the simulated hurricane. The forecasts with bogus data and/or satellite data assimilation (BG and BGSAT) produced a much improved prediction of the recurvature and the subsequent eastward movement that occurred between 42 and 76 h. The BGSAT forecast performed similarly to that of the BG forecast for the hurricane track before 42 h of model integration. After 42 h, the hurricane track in BGSAT was closer to the best track than that of BG. The hurricane tracks before 42 h were located to the east of the observed track in

TABLE 4. The rms errors of the 12-h forecasts when compared with two radiosondes west of the Appalachian Mountain ridge.

Experiment	Fit to data			
	T (°C)	u (m s^{-1})	v (m s^{-1})	q (kg kg^{-1})
	Radiosonde station A			
BG	1.11	3.16	2.72	5.74
BGSAT	0.97	2.72	2.38	5.62
	Radiosonde station B			
BG	1.04	3.29	3.06	3.30
BGSAT	0.73	2.82	2.28	3.59

TABLE 5. The rms errors of the 12-h forecasts when compared with all the radiosonde data available in domain B.

Experiment	Fit to data			
	T (°C)	u (m s^{-1})	v (m $^{-1}$)	q (kg kg^{-1})
BG	1.66	3.41	3.86	4.29
BGSAT	1.42	3.40	3.65	4.25

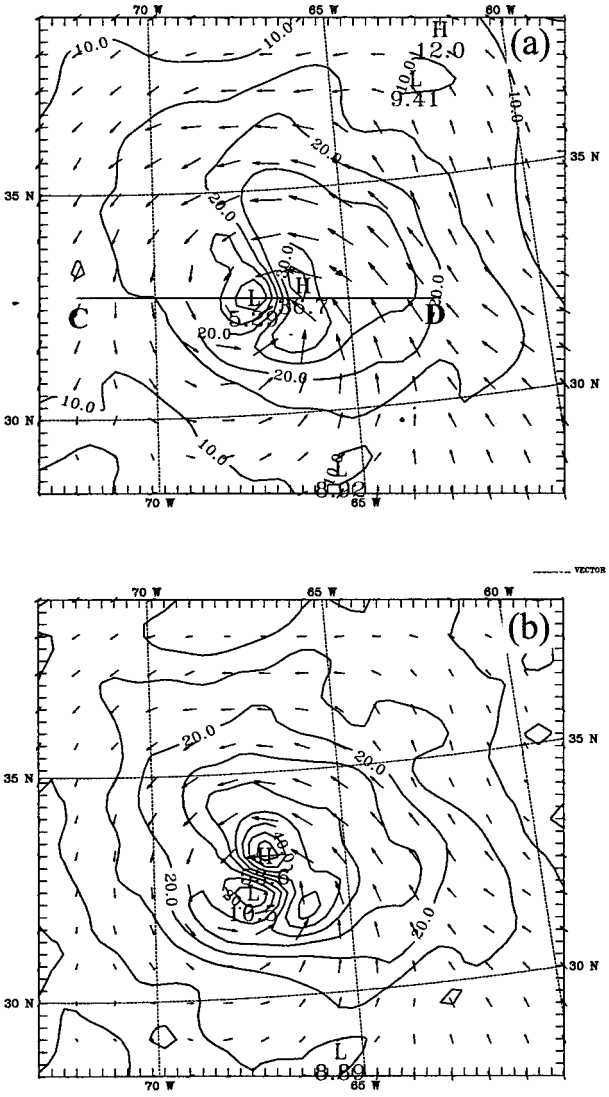

FIG. 12. Distributions of the low-level wind (σ = 0.995) in the (a) BG vortex and (b) BGSAT vortex. The contour interval is 5 m s^{-1}.

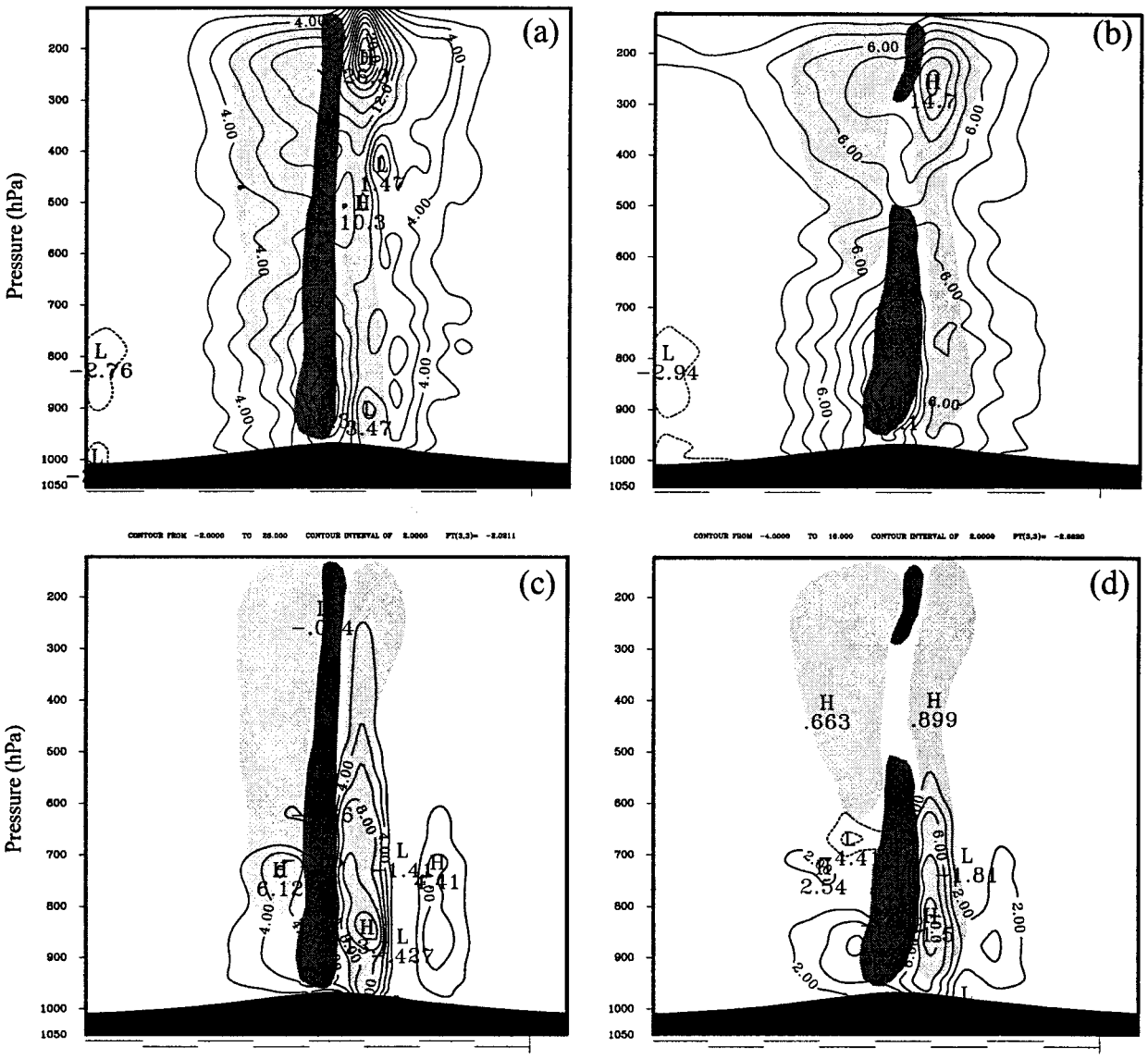

FIG. 13. Cross sections of the adjustment of initial temperature in (a) BG and (b) BGSAT, and the adjustment of initial specific humidity in (c) BG and (d) BGSAT along the line C–D in Fig. 10a. The temperature and specific humidity intervals are 2 K and 2 g kg^{-1}, respectively. Light shading area represents downward motion for which the vertical velocity was less than -15 cm s^{-1}, and the dark shading area represents upward motion for which the vertical velocity was greater than 15 cm s^{-1}.

both BG and BGSAT. Further study is needed to identify the possible cause.

The central SLP and maximum low-level wind were predicted similarly well by BG and BGSAT (Table 6 and Fig. 15), except that during the initial 6 h both BG and BGSAT experienced a spinup time to adjust the imbalance between SLP and wind. BGSAT had a stronger maximum low-level wind at the initial time than the observation. This result suggests that the model's fit to satellite data outside induced some imbalances between wind and temperature into the initial vortex. The SLPs predicted by BG and BGSAT at 1800 UTC 15 August 1999 (the first 6-h model integration) were 952 and 968 hPa, respectively. The latter is closer to the observed value of 966 hPa. In addition, BG is characterized by an extremely large amount of precipitation that occurred at the initial time. The 6-h accumulated rainfall was 375 mm in BG but was substantially reduced to 174 mm in BGSAT. Another noticeable feature in the intensity forecast is that the simulated hurricane in BGSAT is consistently weaker than that of BG during the entire forecast period.

Hurricane Felix made its northward turning from its northwest track between 1800 UTC 16 and 0600 UTC 17 August 1995, and then turned northeastward and later eastward after 0600 UTC 17 August 1995. There was

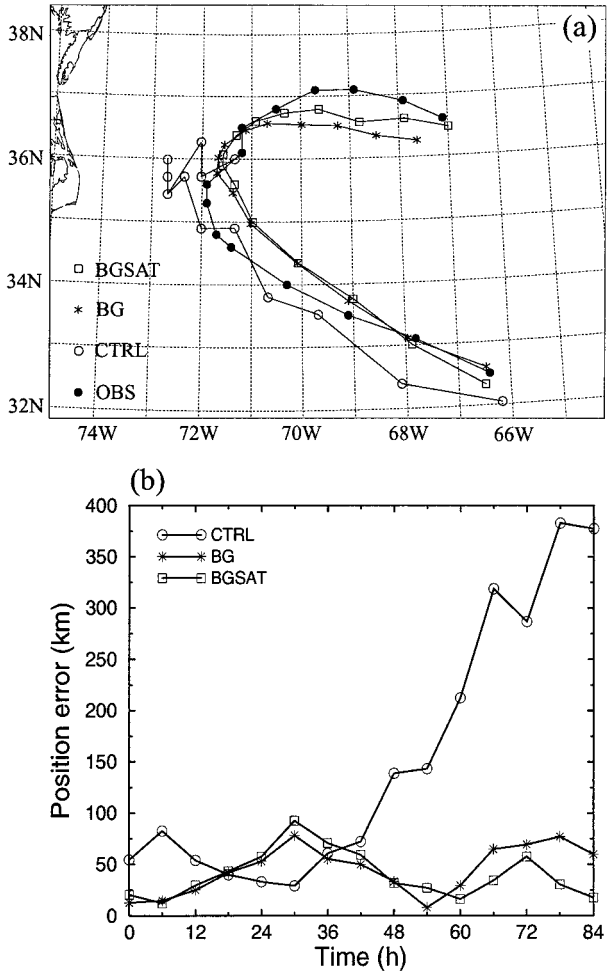

FIG. 14. (a) The observed and simulated Hurricane Felix tracks for the entire forecast period from 1200 UTC 15 to 0000 UTC 19 Aug 1995. (b) The track errors (km).

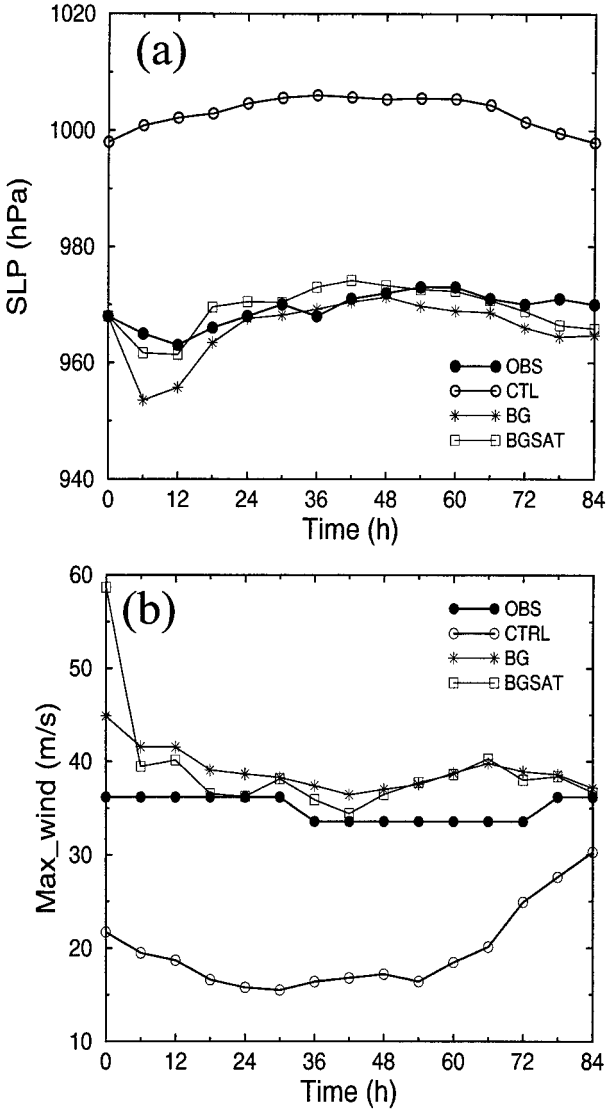

FIG. 15. Time series of (a) the sea level pressure (hPa) and (b) the maximum low-level wind speed (m s^{-1}) from 1200 UTC 15 to 0000 UTC 19 Aug 1995.

an upper-level environmental anticyclonic flow (near 200 hPa) and a low-level synoptic cold front near the east coast of the United States that prevented Hurricane Felix from continuing its northwest track toward landfall.

The difference in the track predictions that occurred around 42–48 h (0600–1200 UTC 17 August) between BG and BGSAT might be related to several factors: (i) the difference in the intensity of the upper-level jet, (ii) the location of maximum latent heat release around the hurricane eye, and (iii) the vertical structure of the simulated Hurricane Felix. Figure 16 shows, for example, the upper-level wind ($\sigma = 0.025$, model level 2, near 200 hPa) from BG (right panels) and BGSAT (left panels) simulations at 1800 UTC 16 and 1200 UTC 17 August 1995 for domain A. We find that the westerly jet west of Hurricane Felix in BGSAT was much stronger than that in BG (Figs. 16c,d). The 15-m s^{-1} isotach to the west of the hurricane in BGSAT intrudes into the hurricane region, but it is located much farther west and away from the hurricane center in BG. We also notice that the hurricane is located in the left jet-exit region in BGSAT and the BG hurricane was located to the east of jet tip. The upper-level westerly jet resulted from the large-scale environmental response to the anticyclonic

TABLE 6. Errors of the 3.5-day forecast of Hurricane Felix.

Experiment	Track		Central SLP		Low-level max wind	
	Mean	Rms errors	Mean	Rms errors	Mean	Rms errors
CTRL	152	197	34	34	−15	16
BG	45	50	−3	5	4	4
BGSAT	40	46	0	3	4	3

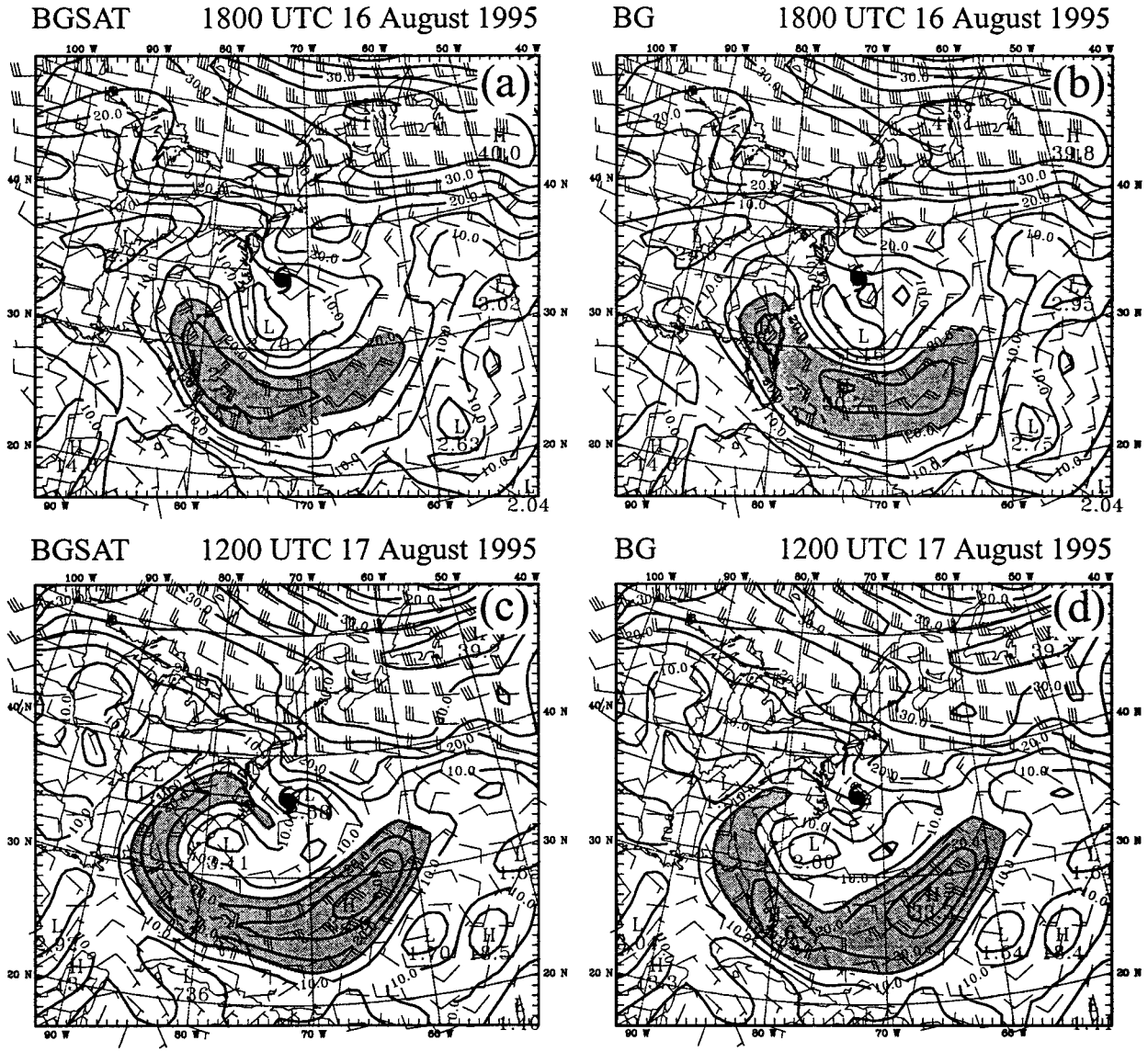

FIG. 16. Wind and isotach (thick line with 5 m s^{-1} interval) at $\sigma = 0.07$ (approximately 200 hPa) on domain A for (a) BGSAT and (b) BG at 1800 UTC 16 Aug 1995, and (c) BGSAT and (d) BG at 1200 UTC 17 Aug 1995. The shaded areas indicate where the wind speed is greater than 20 m s^{-1} in (a) and (b) and greater than 15 m s^{-1} in (c) and (d).

flow that fanned out of the hurricane center and came all the way from the east, south, west, and north, around the immediate environment of the hurricane. The stronger jet in BGSAT was found to be related to the stronger southerly flow that developed between 0000 UTC 16 and 0000 UTC 17 August to the south and southwest of the hurricane (Figs. 16a,b). The latter is related to the initial low-level temperature and moisture changes that resulted from the satellite data assimilation, which extended to upper-level during the course of model integration. Figure 17 shows the temperature distribution at model level 11 ($\sigma = 0.43$, Fig. 17a) and moisture distribution at 850 hPa (Fig. 17b) on domain A for both BG and BGSAT at 1800 UTC 16 August 1995. We find that the cold trough in the upper troposphere (Fig. 17a) was stronger in BGSAT than in BG. This result was found at all the model levels from 9 ($\sigma = 0.35$) to 14 ($\sigma = 0.55$). The differences in the horizontal distribution of the midlevel environmental temperatures increase the thermal gradient of the layer-averaged temperature in the direction from west to east and, thus, increase the meridional wind component (see Fig. 16) based on the thermal wind relation.

We notice that the cooler and drier air started to wrap from the west and southwest of the hurricane at about 1800 UTC 16 August 1995 in BGSAT (Fig. 16), which was delayed to 0000 UTC 17 August in the BG simulation (figure omitted). The cooler air that wrapped

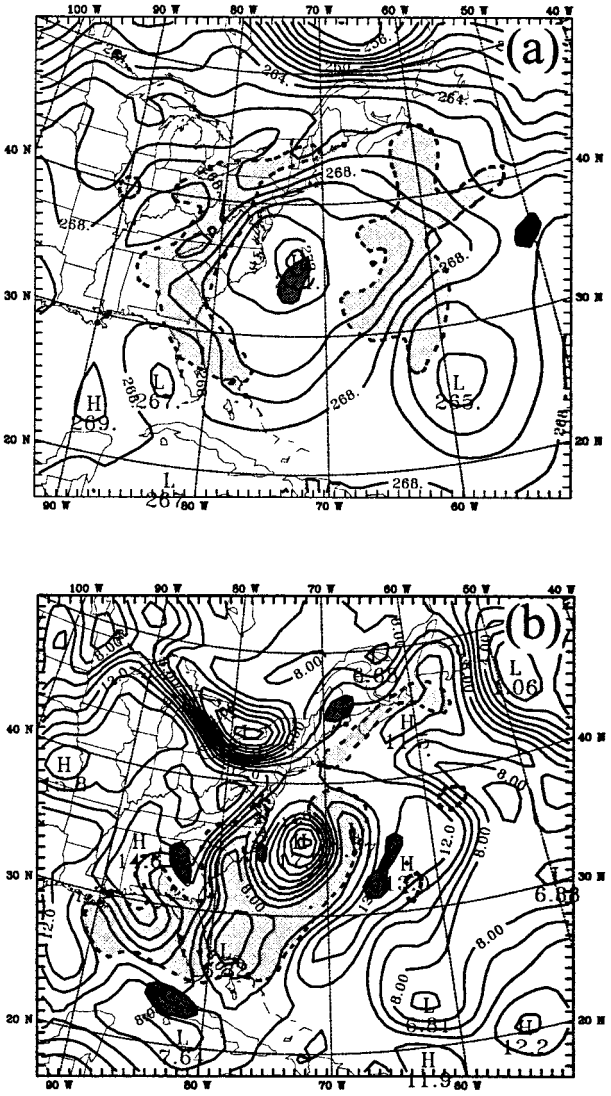

FIG. 17. (a) Temperature distributions in BGSAT (thick line) at $\sigma = 0.43$ at 1800 UTC 16 Aug 1995. Light shading areas with dashed perimeter are areas where the values of temperature difference are less than -0.25 K, and the dark shading areas with solid perimeter are areas where the values of temperature difference are greater than 0.25 K. (b) Same as (a) but for the specific humidity. The intervals for temperature and specific humidity are 1 K and 1 g kg^{-1}, respectively. Light shading areas with dashed perimeter are areas where the values of specific humidity difference are less than -0.5 g kg^{-1}, and the dark shading areas with solid perimeter are areas where the values of specific humidity difference are greater than 0.5 g kg^{-1} at 1800 UTC 16 Aug 1995.

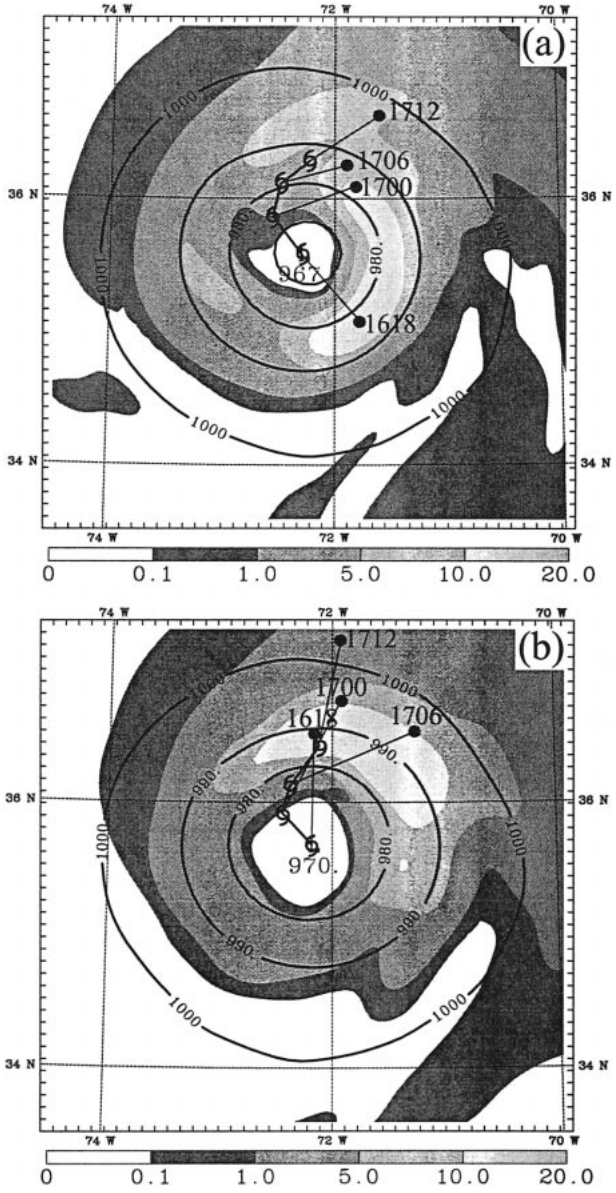

FIG. 18. Vertically integrated model hydrometeors (shading, unit: mm) and sea level pressure (thick line, 5-hPa interval) at 1800 UTC 16 Aug 1995 for (a) BG and (b) BGSAT. The solid dots indicate the centers of the maximum hydrometeors at various times. Each dot is connected to the hurricane center by a thin straight line. The number by each dot (say 1712) indicates the date and time when the centers of the maximum hydrometeors are determined (1712 corresponds to 1200 UTC 17 Aug 1995).

from the west and south of the hurricane in BGSAT was drier than that in BG (see Fig. 17b).

Differences in the predictions of hurricane structures between BG and BGSAT were also found in the location of maximum rainfall and maximum rainwater distributions, and the size of the hurricane eye reflected in the hurricane cloud patterns inferred from the vertically integrated hydrometeor fields or rainfall distributions. An example is shown in Fig. 18, which plots the vertically integrated hydrometeor fields at 1800 UTC 16 August 1995. The maximum vertically integrated hydrometeor fields in BGSAT at various times were found to be located mostly to the north of the hurricane center during the recurving period (1800 UTC 16 to 1800 UTC 17 August 1995, see Fig. 18). In the BG forecast, it was located to the east or slightly east-northeast of the simulated hurricane center. The 6-h rainfall patterns showed a similar feature. The simulated hurricane eye in BGSAT

(about 90 km) was larger than that in BG (about 60 km) during the entire forecast period of 3.5 days. When compared with the size of the observed eye (90–130 km), the simulation of BGSAT is more realistic than that of BG. Such a difference in the mesoconvective scale precipitation and cloud distributions explains the difference in the hurricane intensity forecasts (see Fig. 15a) between BG and BGSAT. The smaller hurricane eye permits the low-level high angular momentum to advance closer toward the storm's center than a larger hurricane eye would allow (Krishnamurti et al. 1998a,b), which results in a slightly stronger intensity forecast, as in the case of BG. This effect is confirmed by the differences of the central SLP values between BG and BGSAT during the entire forecast period (Fig. 15a). We believe that the latent heat release associated with moisture convergence processes contributed to the larger northward component in the BGSAT hurricane track prediction after 1800 UTC 16 August. The BGSAT hurricane track was located farther north than the BG hurricane track (see Fig. 14), more in agreement with the observed track.

The difference in the regions of maximum convection may be associated with the differences in upper-level jet intensity, mentioned before. An interesting difference between BG and BGSAT is in the distributions of the streamline, the temperature, and the wind directions at various levels. Prior to 1800 UTC 16 August, the warm center coincided with the hurricane SLP center and with the cyclonic circulation around the eye at all vertical levels in both BG and BGSAT (not shown). At 1800 UTC 16 August, the warm anomaly and the circulation center were collocated only between 300 and 850 hPa, but not at other levels. Figure 19, for example, shows these distributions at 200 hPa at 1800 UTC 16 (Figs. 19a,b) and 0600 UTC 17 August 1999 (Figs. 19c,d). In BGSAT, the upper-level cyclonic circulation center collocated neither with the warm center nor with the SLP center, but shifted to the northeast at 1800 UTC 16 August (Fig. 19b). Similar features were found at 0000 UTC 17 August (not shown). In BG at 1800 UTC 16 August the cyclonic circulation at 200 hPa still coincided with the low-level hurricane center (indicated by a star sign), and the warm center was only slightly behind the hurricane circulation center, considering the hurricane moved in the northwest direction at that time (Fig. 19a). At 0600 UTC 17 August the BG upper-level circulation center had moved to the northeast of the low-level hurricane center and was collocated again with the warm center (Fig. 19c), but in BGSAT the upper-level circulation center continued to lead the low-level hurricane center and the maximum thermal center (Fig. 19d). After 1200 UTC 17 August the hurricane circulation resumed its vertical alignment, but the maximum temperature center still stayed behind the circulation center (not shown). The eastward shift of the temperature maximum center from low levels to upper levels may result from the stronger eastward temperature advection caused by the stronger upper-level jet in BGSAT than in BG. This stronger upper-level jet contributed to an increased vertical shear in BGSAT, which has caused a tilt in the thermal structure of the cyclone. The upper-level cyclonic circulation, which was located to the north of the maximum temperature center, is a result of jet dynamics.

7. Summary and conclusions

The influence of satellite data on the simulation of Hurricane Felix has been assessed by comparing the MM5 model integrations with and without satellite data being included in the BDA hurricane initialization procedure. All model integrations were performed over 84 h, each beginning at 1200 UTC 15 August 1995, to examine the recurvature of Hurricane Felix from its northwest track to an eastward track during 1800 UTC 16 to 1800 UTC 17 August 1995.

An observation operator, which links the atmospheric state to the *GOES-8* brightness temperatures, and the adjoint of the observation operator were developed and linked to the MM5 adjoint model system. The *GOES-8* satellite data were then included in a hurricane initialization scheme (i.e., the BDA scheme) using a bogus surface low. Although the use of a bogus surface low alone generated a reasonable description of dynamic and thermodynamic structures of the initial vortex, which resulted in an improved hurricane track and intensity prediction, the inclusion of satellite brightness temperature data in BDA was found to be influential and beneficial for the hurricane initialization and forecast. Several changes occurred to the model fields at the initial time, including an intensified low-level warm ridge to the west of the hurricane, a decreased amount of water vapor below 500 hPa over most areas for which satellite data were available, and an intensified thermal ridge over the U.S. continent. Even though there were no cloud-free satellite data over the region of the initial vortex, differences between the initial vortices with and without the use of *GOES-8* brightness temperature data indicate a conceptually more realistic vortex structure when satellite data were included than the one obtained using only the bogus data.

Effects of the satellite data on model simulation were reflected in several aspects of the forecast. The 12-h forecast errors were reduced because of the use of these data, when verified by either the satellite data or the radiosonde data. The track forecasts during the northeast recurvature of Hurricane Felix were also improved when satellite data were included in the initialization procedure. Differences in the prediction of Hurricane Felix with and without satellite data were also found in the forecast of the central sea- level pressure, the upper-level jet, and the cold front that prevented Hurricane Felix from continuing its west-northwest track at 1800 UTC 16 August 1995. The upper-level jet to the west of the hurricane around 1200 UTC 17 August, simulated

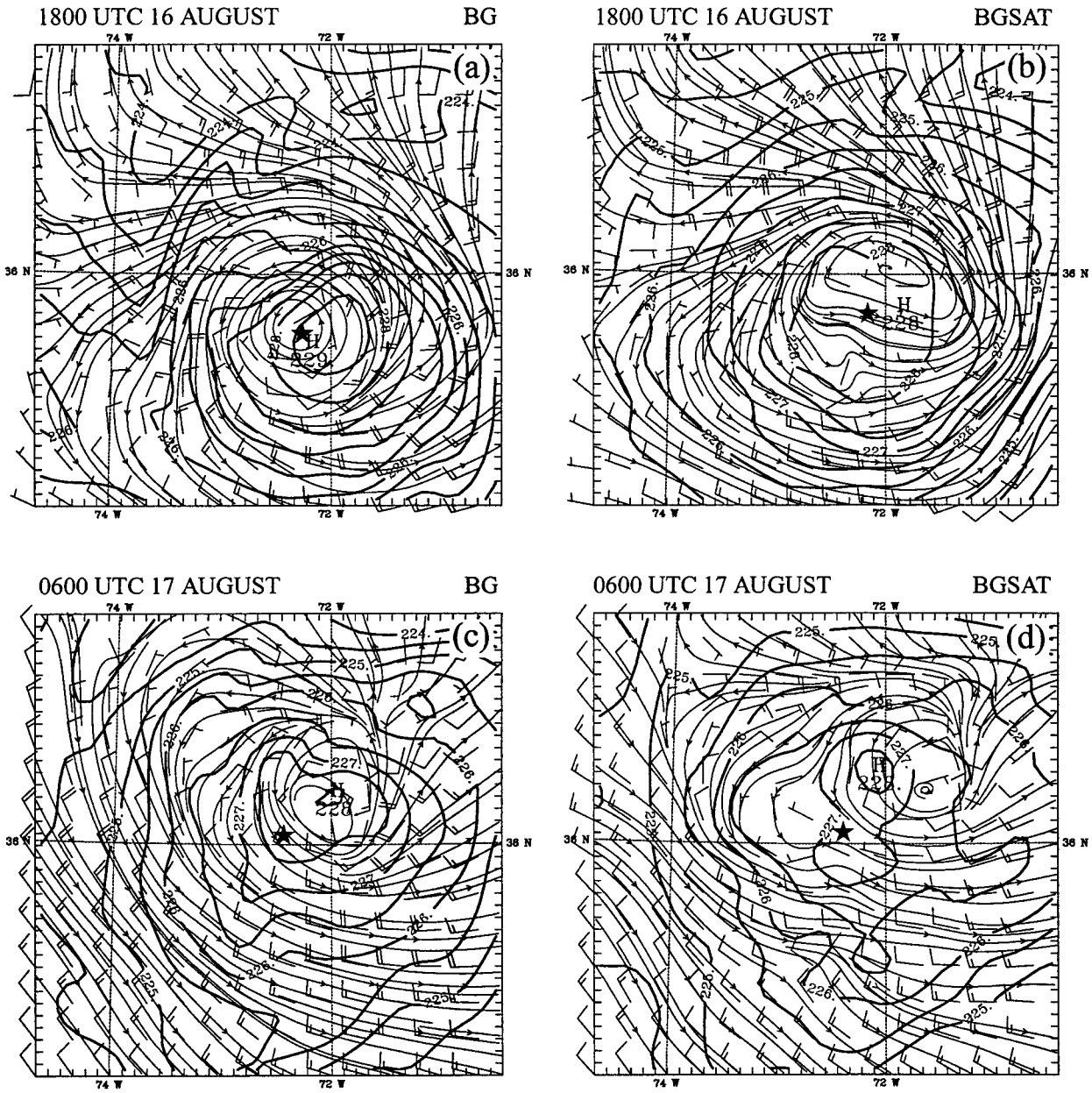

FIG. 19. Wind, streamlines, and temperature distributions (thick line at 0.5 K interval) at 200 hPa from (left) BG and (right) BGSAT at (a)–(b) 1800 UTC 16 Aug 1995, and (c)–(d) 0600 UTC 17 Aug 1995. The simulated hurricane centers are indicated also.

with the use of satellite information, was much stronger than the simulation without using satellite data. The stronger temperature advection and the shifting of the maximum cloud distributions contributed to a larger northward component of Hurricane Felix's movement prior to its eastward turn.

This study identified changes in the prevailing environment through the direct use of *GOES-8* satellite brightness temperature data in a single data assimilation experiment. The modified environment, in turn, influences the storm motion, the storm intensity, the vertical structure of the storm, and the cloud distribution. Numerical results represented serve as an example, showing the potential effect of environmental satellite data on hurricane prediction. The specific differences shown here may vary from case to case and are likely to depend on the particular large-scale environment, as well as the hurricane location, size, structure, and intensity. Although some of the changes in the predictions with and without satellite data are marginal, larger effects are expected with the use of much more satellite data in a data assimilation cycle.

Acknowledgments. The authors thank Donald Hillger for providing the satellite data error analysis method. This research is supported by AFOSR through Project F4920-96-C-0020 and the National Science Foundation under Project ATM-9908939.

REFERENCES

Andersson, E., J. Pailleux, J.-N. Thepaut, J. R. Eyre, A. P. McNally, G. A. Kelly, and P. Courtier, 1992: Use of radiance in 3D/4D variational data assimilation. *Proc. ECMWF Workshop on Variational Assimilation, with Special Emphasis on Three-Dimensional Aspects*, Reading, United Kingdom, ECMWF, 123–156.

Clough, S. A., M. J. Iacono, and J.-L. Moncet, 1992: Line-by-line calculation of atmospheric fluxes and cooling rates: Application to water vapor. *J. Geophys. Res.*, **97,** 15 761–15 785.

Derber, J. C., and W.-S. Wu, 1998: The use of TOVS cloud-cleared radiances in the NCEP SSI analysis system. *Mon. Wea. Rev.*, **126,** 2287–2299.

Dudhia, J., 1993: A nonhydrostatic version of the Penn State–NCAR Mesoscale Model: Validation tests and simulation of an Atlantic cyclone and cold front. *Mon. Wea. Rev.*, **121,** 1493–1513.

Eyre, J. R., 1991: A fast radiative transfer model for satellite sounding systems. ECMWF Research Department Tech. Memo. 176, 28 pp. [Available from European Centre for Medium-Range Weather Forecasts, Shinfield Park, Reading RG29AX, United Kingdom.]

——, and H. M. Woolf, 1988: Transmittance of atmospheric gases in the microwave region: A fast model. *Appl. Opt.*, **27,** 3244–3249.

——, G. A. Kelly, A. P. McNally, E. Andersson, and A. Persson, 1993: Assimilation of TOVS radiance information through one-dimensional variational analysis. *Quart. J. Roy. Meteor. Soc.*, **119,** 1427–1463.

Fleming, H. E., N. C. Grody, and E. J. Kratz, 1991: The forward problem and corrections for the SSM/T satellite microwave temperature sounder. *IEEE Trans. Geosci. Remote Sens.*, **29,** 571–583.

Grell, G. A., J. Dudhia, and D. R. Stauffer, 1994: A description of the Fifth-Generation Penn State/NCAR Mesoscale Model (MM5). NCAR Tech. Note NCAR/TN-398 + STR, 138 pp. [Available from UCAR Communications, P.O. Box 3000, Boulder, CO 80307.]

Hillger, D. W., and T. H. Vonder Haar, 1988: Estimating noise levels of remotely sensed measurements from satellites using spatial structure analysis. *J. Atmos. Oceanic Technol.*, **5,** 206–214.

Karyampudi, V. M., G. S. Lai, and J. Manobianco, 1998: Impact of initial conditions, rainfall assimilation, and cumulus parameterization on simulations of Hurricane Florence (1988). *Mon. Wea. Rev.*, **126,** 3077–3101.

Krishnamurti, T. N., S. K. Roy Bhowmik, D. Oosterhof, and G. Rohaly, 1995: Mesoscale signatures within the Tropics generated by physical initialization. *Mon. Wea. Rev.*, **123,** 2771–2790.

——, W. Han, and D. Oosterhof, 1998a: Sensitivity of hurricane intensity forecasts to physical initialization. *Meteor. Atmos. Phys.*, **65,** 171–181.

——, ——, B. Jha, and H. S. Bedi, 1998b: Numerical simulation of Hurricane Opal. *Mon. Wea. Rev.*, **126,** 1347–1363.

Liou, K.-N., 1980: *An Introduction to Atmospheric Radiation.* Academic Press, 392 pp.

Lipton, A. E., 1998: Improved GOES sounder coverage of cloud-broken data fields. *J. Appl. Meteor.*, **37,** 441–446.

Liu, W.-Y., R. T. Field, R. G. Gantt, and V. Klemas, 1987: Measurement of the surface emissivity of turbid waters. *Remote Sens. Environ.*, **21,** 97–109.

Masuda, K., T. Takashima, and Y. Takayama, 1988: Emissivity of pure and sea waters for the model sea surface in the infrared window regions. *Remote Sens. Environ.*, **24,** 313–329.

Peng, M. S., and S. W. Chang, 1996: Impacts of SSM/I retrieved rainfall rates on numerical prediction of a tropical cyclone. *Mon. Wea. Rev.*, **124,** 1181–1198.

Smith, E. A., and T. F. Lee, 1995: Seventh Conference on Satellite Meteorology and Oceanography. *Bull. Amer. Meteor. Soc.*, **76,** 363–371.

Sutherland, R. A., 1986: Broadband and spectral emissivities (2–18 μm) of some natural soils and vegetation. *J. Atmos. Oceanic Technol.*, **3,** 199–202.

Xiao, Q., X. Zou, and Y.-H. Kuo, 2000: Incorporating the SSM/I-derived precipitable water and rainfall rate into a numerical model: A case study for the ERICA IOP-4 cyclone. *Mon. Wea. Rev.*, **128,** 87–108.

Zou, X., and Q. Xiao, 2000: Studies on the initialization and simulation of a mature hurricane using a variational bogus data assimilation scheme. *J. Atmos. Sci.*, **57,** 836–860.

——, A. Barcilon, I. M. Navon, J. Whitaker, and D. G. Cacuci, 1993: An adjoint sensitivity study of blocking in a two-layer isentropic model. *Mon. Wea. Rev.*, **121,** 2833–2857.

——, Y.-H. Kuo, and Y.-R. Guo, 1995: Assimilation of atmospheric radio refractivity using a nonhydrostatic adjoint model. *Mon. Wea. Rev.*, **123,** 2229–2249.

——, F. Vandenberghe, M. Pondeca, and Y.-H. Kuo, 1997: Introduction to adjoint techniques and the MM5 adjoint modeling system. NCAR Tech. Note NCAR/TN-435-STR, 110 pp. [Available from UCAR Communications, P.O. Box 3000, Boulder, CO 80307.]

——, W. Huang, and Q. Xiao, 1998: A user's guide to the MM5 adjoint modeling system. NCAR Tech. Note NCAR/TN-437+IA, 92 pp. [Available from UCAR Communications, P.O. Box 3000, Boulder, CO 80307.]